



**HAL**  
open science

## Experimental study of caldera formation

Olivier Roche, Timothy H. Druitt, Olivier Merle

► **To cite this version:**

Olivier Roche, Timothy H. Druitt, Olivier Merle. Experimental study of caldera formation. *Journal of Geophysical Research*, 2000, 105 (B1), pp.395-416. 10.1029/1999JB900298 . hal-03031456

**HAL Id: hal-03031456**

**<https://uca.hal.science/hal-03031456>**

Submitted on 10 Dec 2020

**HAL** is a multi-disciplinary open access archive for the deposit and dissemination of scientific research documents, whether they are published or not. The documents may come from teaching and research institutions in France or abroad, or from public or private research centers.

L'archive ouverte pluridisciplinaire **HAL**, est destinée au dépôt et à la diffusion de documents scientifiques de niveau recherche, publiés ou non, émanant des établissements d'enseignement et de recherche français ou étrangers, des laboratoires publics ou privés.



Distributed under a Creative Commons Attribution - NonCommercial - NoDerivatives 4.0 International License

## Experimental study of caldera formation

O. Roche, T. H. Druitt, and O. Merle

Laboratoire "Magmas et Volcans" (UMR 6524 and CNRS), Université Blaise Pascal, Clermont-Ferrand, France

**Abstract.** Scaled experiments have been carried out on caldera collapse mechanisms, using silicone as analogue magma and dry sand as analogue rock. Experiments were carried out in two and three dimensions using a range of roof aspect ratios (thickness/width 0.2 to 4.5) appropriate for caldera collapse. They reveal a general mechanism of collapse, only weakly dependent on the shape of the reservoir. For low roof aspect ratios ( $\leq 1$ ), subsidence starts by flexure of the roof and the formation of outward dipping, reverse ring faults, which in turn trigger formation of peripheral inward dipping, normal ring faults. The subsidence always occurs asymmetrically. In cross section the reverse faults delimit a coherent piston, bounded on each side by an annular zone of inwardly tilted strata located between the reverse and normal ring fault sets. The surface depression consists of a nondeformed area (piston) surrounded by an annular extensional zone (tilted strata). For high aspect ratios ( $> 1$ ), multiple reverse faults break up the roof into large pieces, and subsidence occurred as a series of nested wedges (2-D) or cones (3-D). The extensional zone dominates the surface depression. In the case where preexisting regional faults do not play a major role, the collapse mechanics of calderas probably depends strongly on the roof aspect ratio. Calderas with low roof aspect ratios are predicted to collapse as coherent pistons along reverse faults. The annular extensional zone might be the source of the large landslides that generate intracaldera megabreccias. Collapse into magma reservoirs with high roof aspect ratios may be the origin of some funnel calderas where explosive reaming is not dominant.

### 1. Introduction

Calderas form in a range of terrestrial tectonic settings during large ignimbrite eruptions and by the collapse of shield volcanoes. They also occur on other planets [Wood, 1984]. Caldera diameters range from  $\sim 2$  km to many tens of kilometers. Volumes of erupted products range from a few cubic kilometers to  $> 5000$  km<sup>3</sup> [Williams, 1941; Smith, 1979; Lipman, 1984, 1997].

The subsurface structures and collapse mechanisms of calderas are controversial [Williams, 1941; Reynolds, 1956; Smith and Bailey, 1968; Yokoyama, 1981; Walker, 1984; McBirney, 1990; Scandone, 1990; Branney, 1995; Lipman, 1984, 1997]. The subject is of interest for a number of reasons. Many young calderas are located in densely inhabited areas [Newhall and Dzurisin, 1988]. Post eruptive hydrothermal activity generates economically important ore deposits along caldera faults [Lipman, 1984; Elston, 1994; Ryuba, 1994] and provides a source of geothermal power [Heiken and Goff, 1983; Goff and Gardner, 1988]. The mechanisms of caldera collapse have implications for the dynamics of ignimbrite eruptions [Druitt and Sparks, 1984].

Current models of caldera collapse are based on a combination of field studies, theoretical models, geophysical data, and analogue experimentation. Analogue models are useful because they reproduce aspects of the natural phenomenon on a laboratory scale [Komuro *et al.*, 1984; Komuro, 1987; Martí *et al.*, 1994]. We carried out a series of scaled experiments to

investigate the mechanics of caldera collapse. In the experiments it is the weight of the reservoir roof that drives subsidence, as in real calderas. Our discussion focuses in particular on calderas formed by ignimbrite eruptions [Smith, 1979]. We compare the experimental results with field observations of both young and eroded calderas, and also with structures produced by mining subsidence. Mining subsidence models provide important insights into caldera collapse, but there are major differences in scale. The ratio of subsidence to roof thickness is 10 to 100 times greater in calderas than in mines. Moreover, the difference in scale implies that stresses involved during caldera formation are much greater than in mines. For these reasons, our analogue experiments are scaled to take into account the large dimensions of calderas. The experiments show that many of the caldera collapse geometries proposed in the literature can potentially be explained by a single mechanism. They also have implications for the formation of some funnel calderas and for the dynamics of large ignimbrite eruptions. We begin by reviewing the different models of caldera collapse proposed in the literature.

### 2. Models of Caldera Collapse

Three end-member mechanisms of caldera collapse have been proposed in the literature: piston collapse, noncoherent (chaotic or piecemeal) collapse, and downsag. A fourth type, funnel calderas, is based on caldera morphology, and the exact collapse mechanism is controversial (Figure 1). Individual calderas can in some cases exhibit components of two or more collapse mechanisms.

#### 2.1. Piston Collapse

In the piston collapse model, an essentially coherent block subsides along one or more well-defined ring faults (Figure 1a)

Copyright 2000 by the American Geophysical Union.

Paper number 1999JB900298.  
0148-0227/00/1999JB900298\$09.00

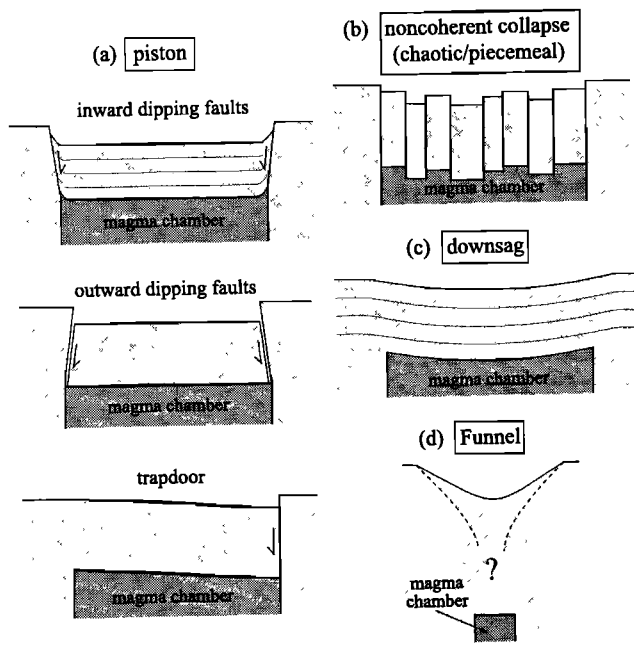


**Figure 1.** Summary of end-member mechanisms of caldera-collapse proposed in the literature. (a) piston models, (b) noncoherent collapse model, (c) downsag model, and (d) funnel model.

[Clough *et al.*, 1909; Williams, 1941; Reynolds, 1956; Smith and Bailey, 1968; Oftedahl, 1978; Lipman, 1984, 1997]. The ring faults are observed directly in eroded calderas [e.g., Oftedahl, 1978, Lipman, 1984]. In young calderas their existence is inferred from alignments of vents along curved arcs [Williams, 1941; Smith and Bailey, 1968; Bacon, 1983; Hildreth and Mahood, 1986; Lipman, 1984]. The piston is often plate-like in geometry and more or less cylindrical. In some cases there are multiple ring faults, such as at Clut caldera [Hildebrand, 1984], Grizzly Peak [Fridrich *et al.*, 1991], Washburn, Pueblo, Long Ridge [Rytuba and McKee, 1984], and La Primavera [Mahood, 1980].

The diameters of calderas interpreted as piston structures range from <10 km, such as Crater Lake [Bacon, 1983], Kulshan [Hildreth, 1996], Ischizuki [Yoshida, 1984], Ischia [Tibaldi and Vezzoli, 1998], and Vepe [Nappi *et al.*, 1991], to considerably more than 10 km, such as Lake City and Silverton [Lipman, 1976], Grizzly Peak [Fridrich *et al.*, 1991], Valles [Smith and Bailey, 1968], Questa [Lipman, 1983], Creede [Steven and Lipman, 1976], Long Valley [Hildreth and Mahood, 1986], Organ [Seager and McCurry, 1988], and Hechiceros [Ritter and Cepeda, 1991]. The amount of subsidence is usually estimated from the thickness of intracaldera tuff and ranges up to 3 km [Smith, 1979; Spera and Crisp, 1981; Lipman, 1984] or, rarely, up to 5 km [John, 1995, Oftedahl, 1978; Seager and McCurry, 1988].

Three different end-member collapse geometries have been proposed for piston calderas: inward dipping ring faults, vertical or outward dipping ring faults, and trapdoor. The existence of inward dipping ring faults has been invoked widely in the literature [Kingsley, 1931; Reynolds, 1956; Smith and Bailey, 1968; Vincent, 1970; Lipman, 1984], but there is an obvious space problem for the subsiding block. Such faults are, in fact,

rarely observed in the field, and in most cases the ring fault dips are very steep or vertical, such as at Lake City [Lipman, 1976], Summitville [Lipman, 1975], Grizzly Peak [Fridrich *et al.*, 1991], and Tavua [Setterfield *et al.*, 1991]. More often, the inward dip is deduced from updrag of strata at the block margins (see Figure 1a) [Kingsley, 1931; Reynolds, 1956; Vincent, 1963, 1970; Oftedahl, 1978; Yoshida, 1984; Simkin and Howard, 1970]. In some cases, complex structures are invoked to accommodate the space problem [Hildebrand, 1984]. It is commonly implied that precollapse tumescence creates inward dipping faults that are then reactivated during subsidence [Smith and Bailey, 1968; Vincent, 1970; Komuro *et al.*, 1984; Komuro, 1987; Gudmundsson, 1988; Gudmundsson *et al.*, 1997]. However, it is geometrically impossible for relaxation of tumescence along inward dipping faults to result in 3 km or more of subsidence. In fact, evidence for precursory tumescence is elusive at most calderas [Lipman, 1984].

Vertical to outward dipping ring faults and ring dikes have been described from the deeper levels of some eroded calderas, such as Ischizuki (70° to 80°) [Yoshida, 1984], Baerum [Oftedahl, 1978], calderas of the Stillwater range [John, 1995], and the Scottish Hebrides [Richey, 1932]. In this case, there is no space problem for the subsiding block. Seismic data at Rabaul show the existence of a shallow-level ring fault with an outward dip of 45° to 80° [Mori and McKee, 1987; Jones and Stewart, 1997]. On a smaller scale the pit craters of Masaya volcano subsided along faults with outward dips of 70° to 80° [Rymer *et al.*, 1998]. Anderson [1936] showed that underpressuring of a magma chamber would lead to subsidence along outward dipping faults. Magma injection along the faults would generate ring dikes.

Some piston calderas subside in an asymmetric, or trapdoor, manner, as commonly deduced from thickness variations of the intracaldera tuff. Examples include Silverton [Steven and Lipman, 1976], Bonanza [Varga and Smith, 1984], Mule Creek [Elston, 1984], Organ [Seager and McCurry, 1988], Grizzly Peak [Fridrich *et al.*, 1991], Tarso-Voon [Vincent, 1963], Fernandina [Simkin and Howard, 1970], and Snowdon [Howells *et al.*, 1986]. At Snowdon the point of maximum subsidence is located near the main eruptive vent, as recognized by a concentration of co-ignimbrite lag breccias.

## 2.2. Noncoherent Collapse

In some calderas the piston does not remain intact during subsidence (Figure 1b). This is called noncoherent, piecemeal, or chaotic collapse. During subsidence of the Scafell caldera the floor broke up into multiple 0.1 to 2 km blocks separated by large faults [Branney and Kokelaar, 1994]. A reinterpretation of the multicyclic Glen Coe caldera indicates that collapse probably occurred in a similar manner [Moore and Kokelaar, 1997, 1998]. The random distribution of postcollapse vents in some calderas such as Campi Flegrei and Hakone [Walker, 1984] may record breakup of the subsided block. The existence of regional fault networks may favor noncoherent collapse at many calderas. In all likelihood, there exists a spectrum of calderas from those in which there is minor breakup of the piston during subsidence to those in which collapse is strongly noncoherent. In practice, it may be hard to distinguish syncollapse faulting from that generated during postcollapse resurgence, as at Valles [Heiken *et al.*, 1990] and Campi Flegrei [Orsi *et al.*, 1996].

The concept of chaotic collapse was used by Scandone [1990] to explain the negative gravity anomalies associated with many

ignimbrite calderas. Scandone supported his hypothesis by reference to collapse in nuclear explosion cavities. However, there is a scale difference of 2-3 orders of magnitude between nuclear cavities and large calderas [Yokoyama and De la Cruz-Reyna, 1991], so the analogy is not valid. It has been proposed that some funnel calderas form by chaotic collapse [Kuno et al., 1971; Aramaki, 1984; Kamata, 1989].

**2.3. Downsag**

In the downsag conceptual model a significant component of the subsidence occurs by flexure (Figure 1c). This was proposed for Taupo caldera by Walker [1984] and the Bolsena calderas by Walker [1984] and Nappi et al. [1991]. However, in these, and most other examples, the evidence for pure downsag is lacking. At most calderas, field data suggest that downsag acts together with faulting to accommodate the subsidence. This is the case for calderas such as those of the Ossipe Mountains [Kingsley, 1931], Ischizuki [Yoshida, 1984], Tavua [Setterfield et al., 1991], Fernandina [Simkin and Howard, 1970], and for the pit craters of Masaya volcano [Ryme et al., 1998]. Downsag is revealed by the existence of surface extensional and compressional features. This is the case at Olympus Mons where, a transition exists between an extensional zone (arcuate grabens) near the caldera margin and a compressional zone (ridges) near the center [Mouginis-Mark and Robinson, 1992]. Arcuate grabens have also been observed at Black Bear [Hildebrand, 1984] and at the Galapagos calderas [Geist et al., 1994]. At Glen Coe, extension caused by downflexure generated surface crevasses hundreds of meters deep at the caldera margins [Moore and Kokelaar, 1997].

**2.4. Funnel Calderas**

Yokoyama [1981, 1983] introduced the concept of funnel calderas. This model differs from the others in that it is based on caldera morphology, rather than on collapse mechanism (Figure 1d). Drill core data and U-shaped negative gravity anomalies suggest that some calderas consist of a flared, funnel-shaped depression filled with breccia. This interpretation has been applied generally to small-diameter (<2-4 km) calderas but also, more rarely, to larger calderas such as Aira [Yokoyama, 1961; Aramaki, 1984], Aso [Ono et al., 1992], La Primavera [Yokoyama and Mena, 1991], and Kuttayaro [Yokoyama, 1983]. Comprehensive drilling at Hakone [Aramaki, 1992], Shishimuta [Kamata, 1989, 1992], and Nigorikawa [Ando et al., 1992; Aramaki, 1992; Kurozumi and Doi, 1994, 1995] has shown that in each case the width of the breccia fill decreases downward. The present experiments may have implications for the origins of some funnel calderas, as discussed in section 9.3.

**3. Previous Experimental Studies of Caldera Formation**

Ramberg [1981] carried out centrifuge experiments using putty (the magma chamber) placed under a roof of clay. Preexisting vertical fractures were generated artificially in the clay, and these guided the subsiding block without creation of other faults. Komuro et al. [1984] used a rigid, upward moving sphere in a volume of clay or in a mixture of sand and clay to simulate the doming created by an ascending magma body in the crust. This produced a depression at the center of the dome that might represent a caldera. Komuro [1987] used an evaporating sphere of dry ice buried in sand and clay and showed that

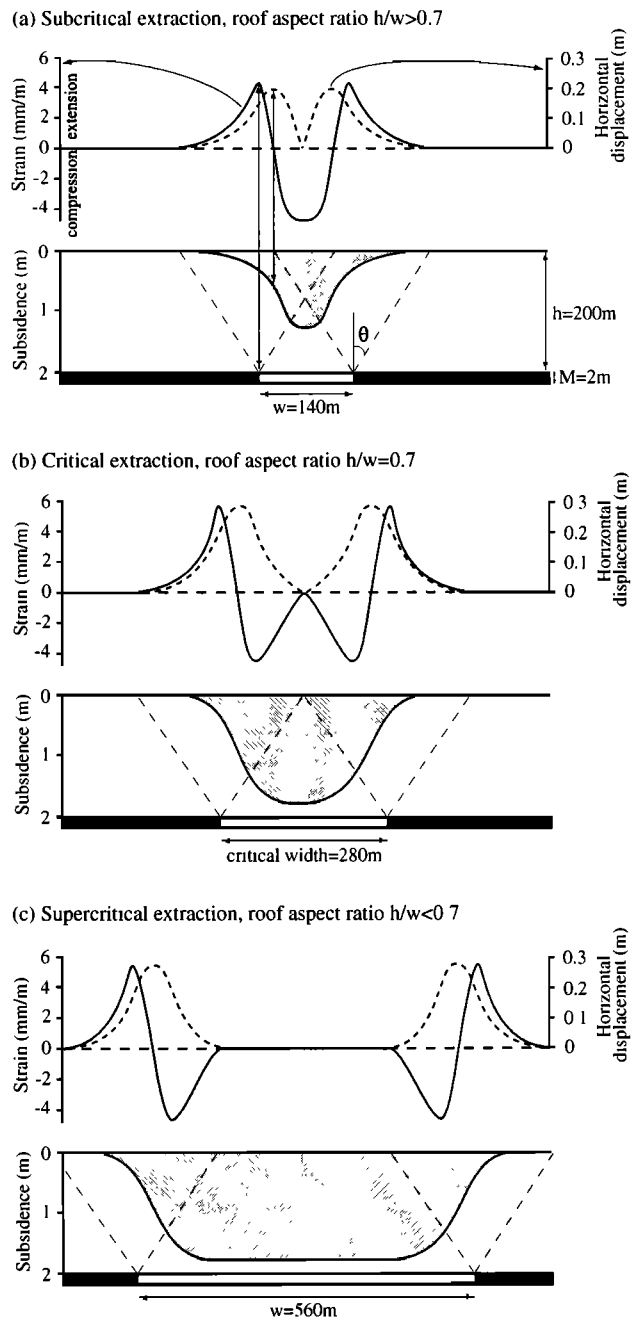


**Figure 2.** National Coal Board [1975] model for subsidence, horizontal displacement, and strain at the surface caused by a rectangular cavity 2 m high and 200 m deep. (a) Subcritical case, (b) critical case, and (c) supercritical case. The angle of draw  $\theta$  is 35°. Maximum horizontal displacement toward the center corresponds to the transition between extensional and compressional strain. The maximal extension occurs above the cavity margins. Modified from Whittaker and Reddish [1989].

collapse occurred as a coherent, subsiding block delimited by outward dipping faults. Martí et al. [1994] used an air balloon immersed in a volume of alumina powder. In their experiments the balloon was inflated to simulate pre-collapse tumescence and/or deflated to simulate syneruptive collapse. Reverse, inward dipping faults generated during tumescence seemed to reactivate during subsidence when the balloon was deflated. For subsidence

alone, collapse took place as a block delimited by vertical faults and cut internally by a complex pattern of curved faults. A limitation of these experiments is that during subsidence a balloon conserves its upward convex shape and imposes deformation on the roof, not the contrary as in a caldera.

#### 4. Principles of Subsidence Mechanics

The basic principles of subsidence mechanics are well known from mining subsidence studies [Vidal, 1961; Given, 1973; National Coal Board, 1975; Whittaker and Reddish, 1989; Hoek et al., 1995]. Subsidence in mines is small compared to the thickness of the mine roof. For example, typical subsidences are less than a few meters, whereas the roof thickness is several hundreds of meters (Figure 2). The ratio of subsidence to roof thickness is about  $10^{-2}$  in mines and 10 to 100 times greater in many calderas.

The National Coal Board [1975] published an empirical model widely used for subsidence prediction [Whittaker and Reddish, 1989]. For two-dimensional subsidence, two lines drawn from the edges of the cavity delimit the collapse depression at surface (Figure 2). The angle  $\theta$  between these lines and the vertical is called the angle of draw and is equal to  $-35^\circ$ . Subsidence at the surface is accompanied by horizontal displacements at the surface toward the center of the depression. At the center of the system, there is no horizontal displacement. Horizontal displacements cause formation of both extensional and compressional zones at the surface (Figure 2). The points of maximum extension are located above the edges of the cavity. The transition between the zones of surface extension and compression corresponds to the maximum gradient of subsidence. The National Coal Board [1975] model distinguishes three cases depending on the roof aspect ratio ( $R$ =thickness/width): subcritical, critical, and supercritical. The critical aspect ratio (Figure 2b) is given by

$$\tan\theta = (w/2)/h = 1/(2R), \quad (1)$$

where  $w$  and  $h$  are the width and thickness of the roof, respectively. For  $\theta=35^\circ$  we obtain a critical aspect ratio of  $R=0.7$ . For  $R>0.7$  (subcritical case, Figure 2a), there is a single point of maximum compression located at the center of the depression. For  $R=0.7$  (critical case, Figure 2b), there are two points of maximum compression and a single point of no deformation at the centre. For  $R<0.7$  (supercritical case, Figure 2c), there are two points of maximum compression and an undeformed zone of finite width in between. The model shows that the widths of the marginal deformed zones (extensional plus compressional) are constant for a given  $\theta$  and  $h$ , and do not depend on  $w$ . This implies that for a low  $R$ , there is a central undeformed zone

bounded by marginal deformed zones, whereas for a high  $R$  the entire depression is affected by surface deformation. The concept of critical aspect ratio is important in our experiments.

#### 5. Experimental Methods

The experiments used dry sand as an analogue for rock and silicone as analogue magma (Table 1). The use of sand to mimic the brittle behavior of rock has been widespread since Hubbert's [1937, 1951] studies. Dry sand has a Mohr-Coulomb behavior and is cohesionless. The sand used in the experiments has a bulk density of  $1500 \text{ kg m}^{-3}$  and a grain size of 60 to  $300 \mu\text{m}$ , with a mean diameter of  $200 \mu\text{m}$ . The angle of internal friction  $\phi$  ( $33.5 \pm 0.8$ ) was estimated from 64 measurements of the angle of repose. Drying the sand does not change its physical properties. Silicone putty is a Newtonian fluid with a viscosity of  $2.4 \times 10^4 \text{ Pa s}$ , as measured using a rotating viscometer. Its density is  $1150 \text{ kg m}^{-3}$ . Gradients in rock properties (e.g., due to temperature variations) and magma viscosity (e.g., due to compositional zoning) were neglected in the experiments.

The experiments were carried out in both two and three dimensions (Figure 3). In each case a layer of silicone (hereinafter referred to as the silicone reservoir) represented the magma chamber. This was underlain by a large volume of silicone connected to an outflow tube, which was blocked during the preparation phase of each experiment. The silicone reservoir was created using a mould of appropriate shape, then was buried and overlain by layered, colored sand that simulated the chamber roof. Each experiment was initiated by unblocking the outflow tube, allowing silicone to flow out of the reservoir, pushed by the subsiding roof. The 2-D apparatus ( $60 \times 10 \times 30 \text{ cm}$ , Figure 3a) was used to understand the basic mechanisms of subsidence. The 3-D apparatus ( $60 \times 60 \times 30 \text{ cm}$ , Figure 3b) was then used to verify the mechanisms observed in two dimensions and to study details of fault propagation and surface deformation in three dimensions.

Silicone reservoirs in the 2-D experiments were rectangular in cross section with vertical sides and flat roofs. Many granite plutons are believed to have approximately flat roofs [Pitcher, 1978; Lipman, 1984; Takahashi, 1986; Lipman et al., 1993; Fiske and Tobbish, 1994; John, 1995]. In the 3-D experiments we first used cylindrical reservoirs with flat roofs; we subsequently investigated collapse into reservoirs of more complex geometry. The range of investigated roof aspect ratios ( $R = 0.2$  to  $4.5$ ) corresponds to that likely in calderas.

After each experiment the model was covered with sand to preserve the depression and other surface structures. The model was then saturated with water and serially sectioned. In some cases, dilute soap solution was used to reduce the surface tension

**Table 1.** Values of the Physical Parameters in Experiments and Calderas in Nature

Parameter	Density $\rho$ , $\text{kg m}^{-3}$	Gravity Acceleration $g$ , $\text{m s}^{-2}$	Typical Length $L$ , $\text{m}$	Stress $\sigma = \rho g L$ , $\text{Pa}$	Angle of Internal Friction $\phi$ , $\text{deg}$	Viscosity $\eta$ , $\text{Pa s}$
$X_{\text{model}}$	1500	10	$o(10^{-2})^a$	150	34	$2.4 \times 10^4$
$X_{\text{nature}}$	2700-3000	10	$o(10^3)$	$2.7 \times 10^7$ to $3 \times 10^7$	25-40	$10^2$ - $10^6$
$X^* = X_{\text{model}}/X_{\text{nature}}$	$\sim 0.5$	1	$o(10^{-5})$	$\sim 0.5 \times 10^{-5}$	$\sim 1$	$o(10^{-2}$ - $10^2)$

<sup>a</sup> The  $o(10^{-2})$  means order of 0.01.

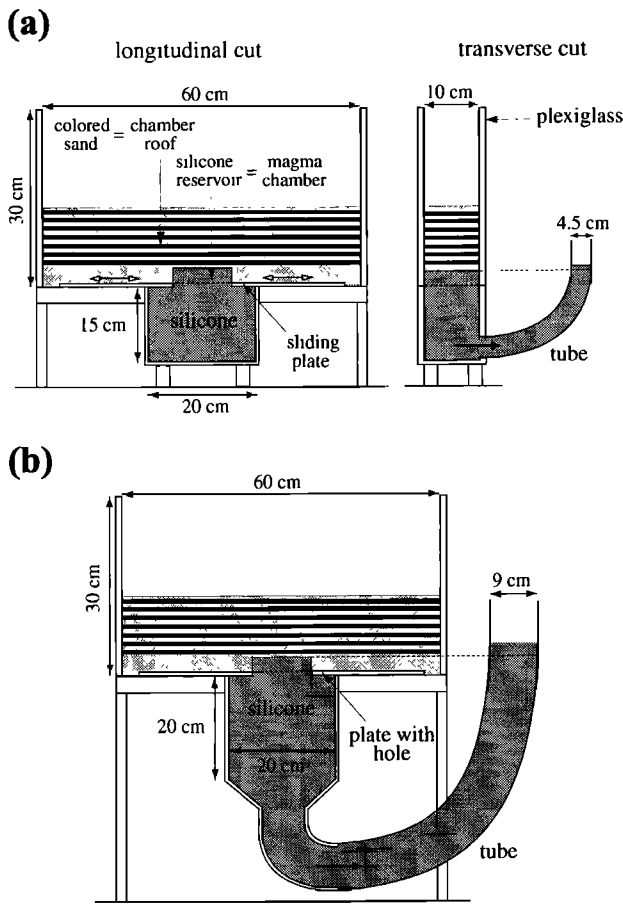


**Figure 3.** Experimental apparatus used in this study. Colored sand mimics the chamber roof. The thin layer of silicone represents the magma chamber. This is referred to as the silicone reservoir in the text. During an experiment the silicone leaves the reservoir via an open tube, driven by the weight of the overlying sand. (a) Two-dimensional apparatus and (b) 3-D apparatus

of water and facilitate penetration into the sand. The experiments are listed in Table 2.

In all the experiments the level of silicone in the open tube was kept above that of the silicone in the apparatus but below that of the top of the sand. It was thus the difference in density between the roof and the silicone that drove the subsidence. Test runs showed that only when the level in the tube lay below that of the apparatus did the silicone flow under its own weight, sucking the sand down with it. Our chosen experimental conditions avoided this effect. Tests were also carried out to confirm the reproducibility of the experiments.

Edge effects in the experiments were unavoidable due to the finite size of the apparatus. This is because vertical stresses ( $\sigma_v$ ) are in part supported by horizontal stresses ( $\sigma_h$ ) against the container walls, where  $\sigma_h = K\sigma_v$ , and  $K$  is a constant equal to 0.58 in sand [Duran, 1997]. In a container full of sand

$$\sigma_v = \rho g \alpha (1 - e^{-h/\alpha}), \quad (2)$$

where  $\rho$  is the bulk density of the sand,  $g$  is the gravitational acceleration, and  $h$  is depth. The constant  $\alpha$  depends on the dimensions of the experimental apparatus:  $\alpha = A/(PK\mu)$ , where  $A$  and  $P$  are the area and perimeter of the apparatus and  $\mu$  is the

coefficient of internal friction (about 0.67). When  $h = 0$ ,  $\sigma_v \approx \rho gh$ , but as  $h$  increases,  $\sigma_v$  tends to a maximum value of  $\rho g \alpha$  (Figure 4). Departures of the vertical stress from lithostatic were less important in the 3-D apparatus than in the 2-D one, in which the maximum deviation was ~40%. However, the similarity of subsidence geometries in two and three dimensions suggest that the resulting effects were of only secondary importance.

### 6. Scaling Considerations

Correct scaling requires geometric and dynamic similarity between the model and nature [Hubbert, 1937, 1951; Sanford, 1959; Ramberg, 1981]. For each key physical parameter we define a ratio  $X^*$  (Table 1) :

$$X^* = \frac{X_{\text{model}}}{X_{\text{nature}}} \quad (3)$$

$L^*$  is the length ratio,  $\rho^*$  is the density ratio,  $g^*$  is the gravitational acceleration ratio, and  $\sigma^*$  is the stress ratio. Calderas have diameters up to several tens of kilometers, subsidences up to 5 km, and magma chamber depths up to ~10 km [Smith, 1979; Spera and Crisp, 1981; Lipman, 1984, 1997; Newhall and Dzurisin, 1988]. We chose a range of  $L^*$  from  $0.5 \times 10^{-5}$  to  $2 \times 10^{-5}$ , so that 1 cm in the experiments corresponded to 0.5 to 2 km in nature. The density ratio  $\rho^*$  in the experiments was ~0.5. The experiments were carried out in the Earth's gravity field, so  $g^* = 1$ . For the scaling of stress parameters,

$$\sigma^* = \rho^* g^* L^* \quad (4)$$

For a Coulomb material like rock or sand,  $\tau = \tau_0 + \sigma_n \tan \phi$ , where  $\sigma_n$  is normal stress,  $\tau$  is shear stress,  $\tau_0$  is cohesion, and  $\phi$  is the angle of internal friction. The angle of internal friction of dry sand (~34°) is in the range (25°-40°) of most rocks [Handin, 1966; Hoek et al., 1995]. To fulfil the scaling condition, with  $\sigma^*$

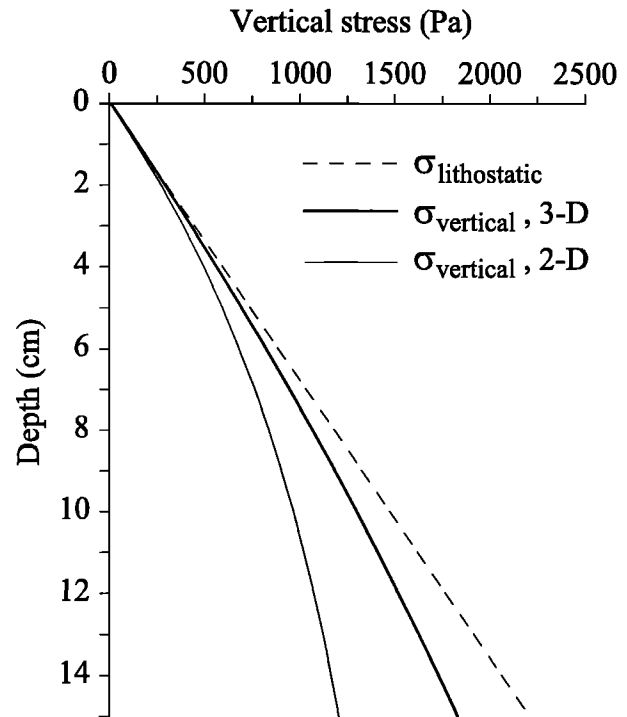


**Figure 4.** Vertical pressure gradients in sand in the 2-D and 3-D experiments. Calculated using equation (2).

**Table 2.** List of Experiments Carried Out in This Study

Experiment	Type	Material <sup>a</sup>	Aspect Ratio <sup>b</sup>	Roof Thickness, <sup>c</sup> cm	Roof Width, <sup>d</sup> cm	Subsidence, <sup>e</sup> cm
5	2-D	sand	0.2	3	15	0.5
7	2-D	sand	0.2	3	15	0.8
6	2-D	sand	0.2	3	15	1.2
3	2-D	sand	0.2	3	15	1.8
12	2-D	sand	1	5	5	0.65
20	2-D	sand	1	5	5	1
22	2-D	sand	1	5	5	1.5
8	2-D	sand	2	10	5	0.2
21	2-D	sand	2	10	5	0.35
4	2-D	sand	2	10	5	1.1
10	2-D	sand	4.5	13.5	3	0
11	2-D	sand	4.5	13.5	3	0.4
9	2-D	sand	4.5	13.5	3	1
32	3-D	sand	0.2	3	15	1.8
34	3-D	sand	0.2	3	15	1.8
45	3-D	sand-flour	0.2	3	15	1.8
35	3-D	sand	0.5	4	8	1.6
36	3-D	sand-flour	0.5	4	8	1.6
38	3-D	sand-flour	1	5	5	1.5
46	3-D	sand	1	5	5	1.5
41	3-D	sand	2	10	5	1.1
43	3-D	sand-flour	2	10	5	1.1
47	3-D, square	sand-flour	0.2	2.8	13.4	1.8
48	3-D, square	sand-flour	2	10	5	1.2
49	3-D, rectangle	sand-flour	0.2	3	7.5x15	1.8
50	3-D, rectangle	sand-flour	2	10	5x10	1.2
53	3-D, ellipse	sand-flour	0.2	2.5	7.5x12.5	1.3
59	3-D, ellipse	sand-flour	2	8	4x8	1.2
52	3-D, hemicylinder	sand-flour	0.2	2	10x16	2
51	3-D, hemicylinder	sand-flour	2	10	5x10	1.4
57	3-D, hemisphere	sand-flour	0.2	1.6	8	1.8
56	3-D, hemisphere	sand-flour	2	10	5	1.2

<sup>a</sup> Material means nature of the upper layer

<sup>b</sup> Aspect Ratio is thickness versus width of the roof

<sup>c</sup> For rounded silicone layer the roof thickness is taken as the thinnest one above the silicone reservoir.

<sup>d</sup> For rounded silicone layer the roof width is the maximum width of the silicone reservoir

<sup>e</sup> Subsidence means maximum collapse at surface.

$= \tau_0^*$ , we have  $\tau_{0,model} = \tau_0^* \tau_{0,nature}$ . Cohesion values for rock measured on small laboratory samples are of the order of  $10^7$  Pa [Handin, 1966, Hoek et al., 1995]. On a larger scale, joints and faults can lower cohesion by at least one order of magnitude [Schultz, 1996]. Thus the macroscopic cohesion is likely to be of the order of  $10^6$  Pa. With  $\tau_0^*$  of the order of  $0.5 \times 10^{-5}$  (Table 1) we need an analogue material with a cohesion of a few pascals. The use of cohesionless dry sand was therefore a good approximation.

Magma viscosities in nature range from  $10^2$  Pa s for basalt to about  $10^6$  Pa s for hydrous rhyolite [Shaw, 1972]. Perfect scaling in our experiments required an analogue fluid much less viscous than silicone. Use of silicone increased the duration of subsidence but did not change the fault geometries created, since the deformation of Coulomb materials is rate-independent. The

high viscosity of the silicone and granular nature of sand prohibited intrusion of the silicone and the formation of "ring dikes" in the experiments.

## 7. Experimental Results

### 7.1. Two-Dimensional Reservoir

In these experiments the silicone reservoir was rectangular with a flat roof and vertical sides. For each roof aspect ratio (0.2, 1, 2, and 4.5) we carried out three or four separate experiments arrested (by blocking the outflow tube) after different amounts of subsidence. By studying the internal structure of each experiment we were able to reconstruct a temporal sequence of fault propagation and collapse for each roof aspect ratio (Figures 5 to

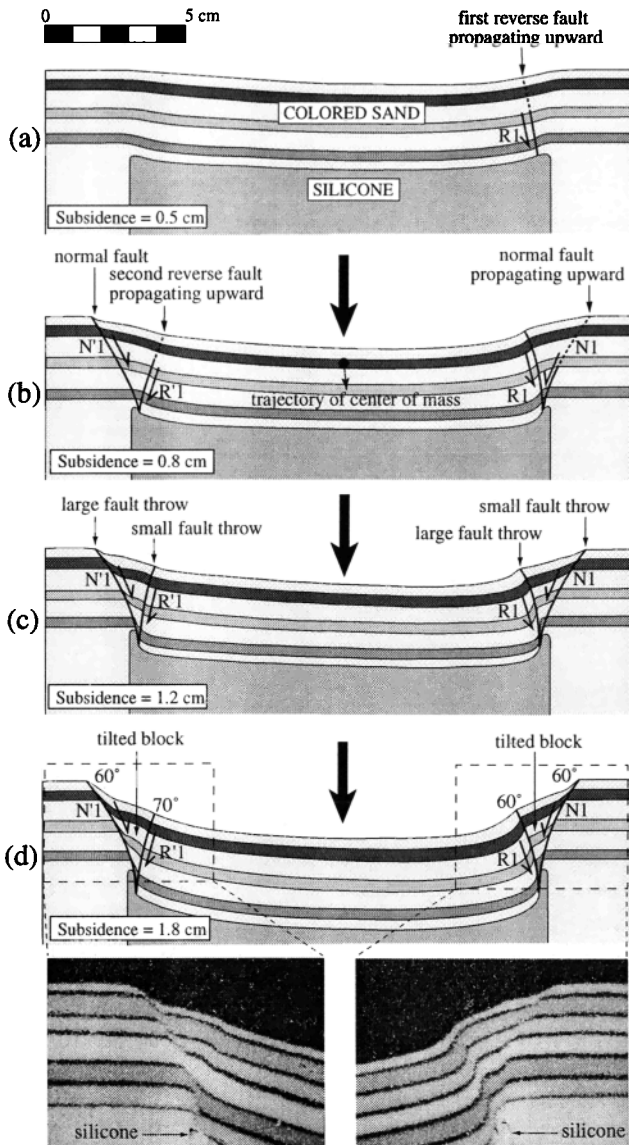


**Figure 5.** Two-dimensional experiments. Roof aspect ratio of 0.2. (a) Experiment 5, (b) experiment 7, (c) experiment 6, and (d) experiment 3. The experiments represent a temporal evolution of the system, arrested at different stages. R, reverse fault; N, normal fault.

8). This was possible because our experiments were reproducible. Subsidence was commonly asymmetric, so in the accompanying diagrams we have for convenience inverted some images so that the asymmetry is always seen in the same sense. Reverse and normal faults are labeled R and N, respectively.

Subsidence in all cases started with downflexure, without the formation of discrete faults. This was most marked at low roof aspect ratios (Figure 5). Further collapse then occurred along a combination of outward dipping reverse and inward dipping normal faults, each of which nucleated at the top of the silicone reservoir and propagated upward (Figures 5 to 8). The faults were subvertical at depth with dips of 55° to 70° (reverse faults) and 60° to 65° (normal faults) at the surface.

At an aspect ratio of 0.2 (Figure 5), nucleation of a first reverse fault (R1) on one side of the reservoir was followed by nucleation of a normal fault (N'1) on the other side. Early subsidence was controlled by these two faults, and the collapse

vector was inclined toward R1. Downthrow along R1 and N'1 then triggered formation of faults R'1 and N1 in a similar manner, and the collapse became more symmetrical. The same took place at an aspect ratio of 1, except that both reverse faults nucleated

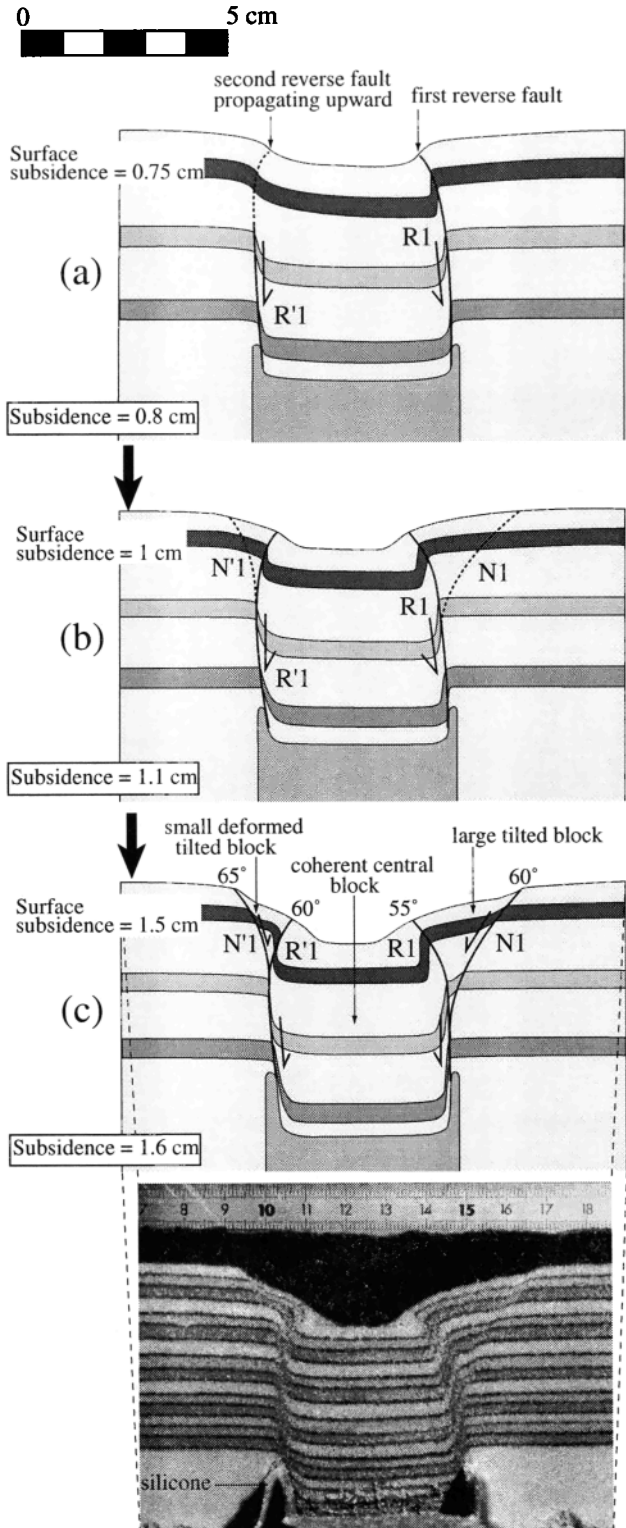


**Figure 6.** Two-dimensional experiments. Roof aspect ratio of 1. (a) Experiment 12, (b) experiment 20, and (c) experiment 22. The experiments represent a temporal evolution of the system, arrested at different stages. The uppermost layer of black sand in the photograph is placed on the model after the experiment to protect the collapse depression. R, reverse fault; N, normal fault.

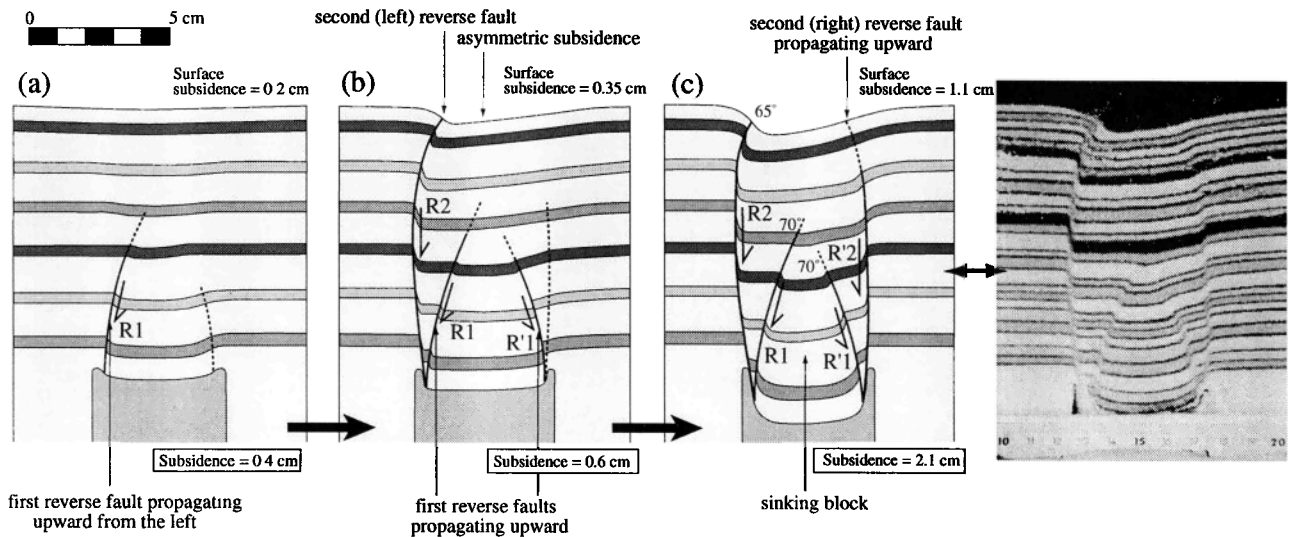


**Figure 7.** Two-dimensional experiments. Roof aspect ratio of 2. (a) Experiment 8, (b) experiment 21, and (c) experiment 4. The experiments represent a temporal evolution of the system, arrested at different stages. The uppermost layer of black sand in the photographs was placed on the model after the experiment to protect the collapse depression. R, reverse fault; N, normal fault.

before the normal ones. In both cases, the reverse and normal faults bounded blocks of strata tilted at 10° to 20° toward the depression (Figures 5 and 6). The reverse faults migrated progressively into these tilted blocks as subsidence occurred (Figure 9). A notable feature of the final structures is the presence of marginal updrag of sand layers along reverse as well as normal faults.

At higher aspect ratios (2 and 4.5) collapse occurred along multiple reverse faults, which broke the roof up into a series of wedges (Figures 7 and 8). In these cases, a first pair of faults (R1

and R'1) nucleated at the top of the reservoir and propagated upward. This triggered formation of a second pair higher up (R2 and R'2), then (for an aspect ratio of 4.5) a third pair (R3 and R'3). Peripheral normal faults were not generated at these aspect ratios. Additional experiments showed that they do eventually form in such systems but only at very large, and geologically unrealistic, subsidences (more than 5 km when scaled).

Despite the use of a very simple geometry for the silicone layer and a roof of constant thickness, only minor departures from symmetry in the initial setup always led to asymmetric

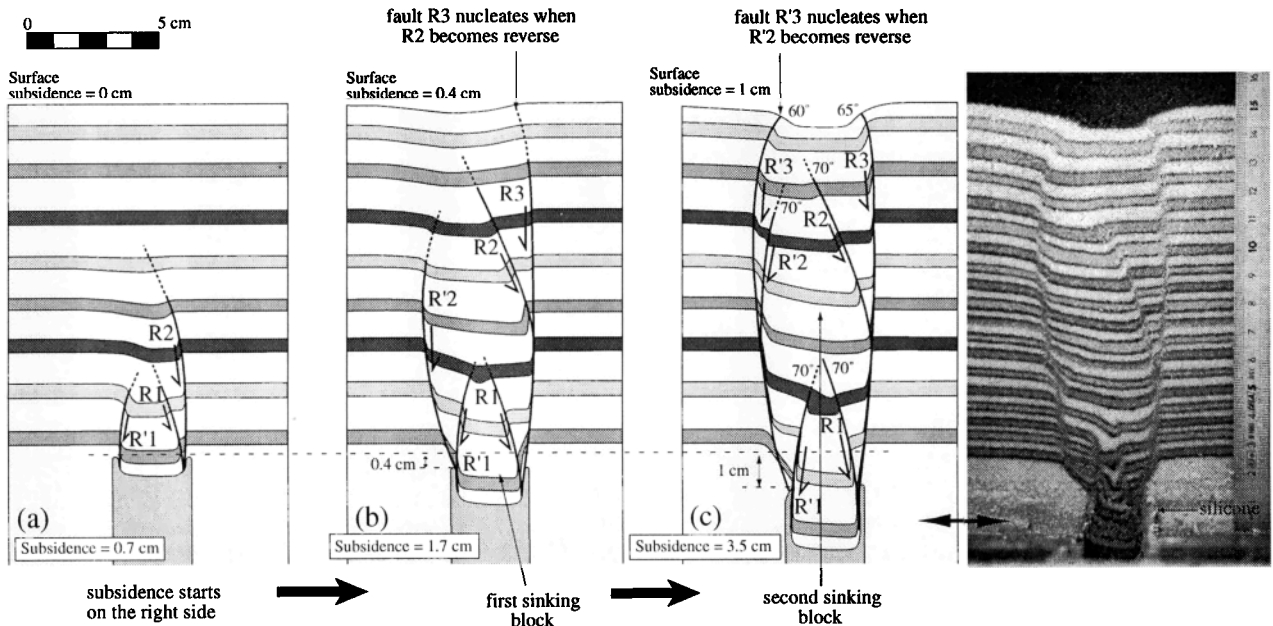


**Figure 8.** Two-dimensional experiments. Roof aspect ratio of 4.5. (a) Experiment 10, (b) experiment 11, and (c) experiment 9. The experiments represent a temporal evolution of the system, arrested at different stages. The uppermost layer of black sand in the photographs was placed on the model after the experiment to protect the collapse depression. R, reverse fault; N, normal fault.

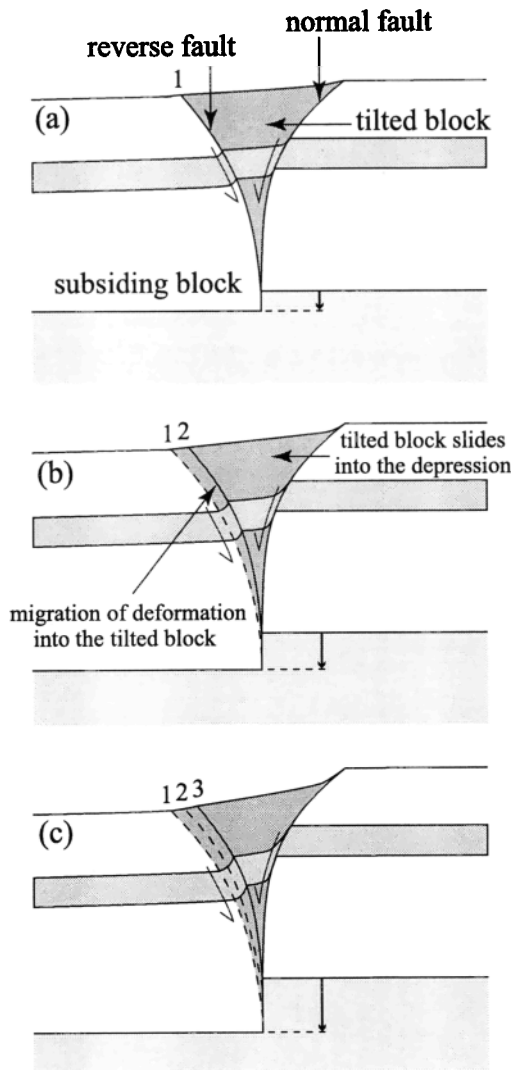


**Figure 9.** Low aspect ratio, 2-D experiment. Migration of reverse fault into the adjacent tilted block during subsidence.

collapse. Tests showed that subsidence always started where the roof was thickest, even subtly so. At the lowest aspect ratio (0.2), subsidence at depth was equal to that at the surface (Figure 5d), whereas at the highest ratio (4.5) the former was >3 times greater. In all experiments, the width of the final surface depression was greater than that of the silicone reservoir. For a given subsidence this effect increased with increasing roof aspect ratio.

**7.2. Three-Dimensional Reservoir (Cylinder With Flat Roof)**

These experiments were carried out to verify the basic mechanisms described above and to study fault propagation and surface deformation in three dimensions. The silicone reservoir was cylindrical with a flat top. Roof aspect ratios of 0.2, 0.5, 1, and 2 were investigated. Following subsidence, the sand was serially sectioned (up to 30 sections, each 0.5 to 1 cm thick) to study internal structures. Timed photographs of the surface during the experiment permitted us to follow each surface fault as it propagated around the deepening depression. The final structures are summarized in Figure 10.

As in two dimensions, the collapse style depended on roof aspect ratio. At low aspect ratios (0.2 and 0.5), subsidence began by flexure, then continued as a coherent piston along reverse and normal ring faults (Figures 11 and 12). An annular ring of strata between the reverse and normal faults was rotated down and into the deepening depression (equivalent to the tilted blocks in two dimensions). In detail, a first reverse fault R1 appeared on one side of the depression and a normal fault N'1 on the other, producing initial asymmetric collapse. Each fault then propagated round the depression through 180°. With increasing subsidence a second reverse fault R'1 appeared and propagated round to meet R1. At the same time, a second normal fault N1 nucleated and propagated round to N'1. In some cases the faults merged totally, forming a complete ring fault (reverse or normal), and in others they crossed at a shallow angle.

At higher aspect ratios, multiple ring faults sliced the subsiding block into a series of cones (Figures 13 and 14). The faults were subvertical at depth and either reverse or normal near the surface. They formed progressively from the bottom to the top, such that in Figure 14, R1 is the oldest and R4 is the youngest. Unlike at lower aspect ratios, each ring fault appeared to nucleate on just one side of the reservoir and propagate all the way round.

Collapse in all cases was asymmetric, with maximum subsidence on the side of the first reverse fault. The dips of reverse faults at the surface ranged from 45° to 85°. In most experiments the dip of each reverse fault became steeper as it propagated around the reservoir. An example is shown in Figure 10a, where R1 has a dip of 50° where it first nucleated, but 80-85° at its lateral extensions. The normal ring faults had almost constant dips (50° to 65°) at the surface but steepened downward. Small secondary normal faults developed between the main reverse and normal fault sets at the lowest aspect ratio (Figure 11).

In some cases a 5-mm-thick layer of sand-flour mixture (cohesion 6 to 8 Pa) was spread uniformly across the surface of the sand prior to the experiment. This made it possible to generate open fractures and to visualize zones of surface extension and compression, which is otherwise not possible with pure sand. The presence of this layer did not influence internal structure or reproducibility in the experiments. It did, however, permit the formation of small vertical cliffs (3 to 4 mm), which scale to several hundreds of meters in nature. These experiments showed that at low aspect ratios the annular ring of tilted strata between the reverse and normal ring faults appears at the surface as an annular zone of extension encircling the non-deformed piston (Figures 11, 12, and 13). The extensional zone also developed at higher aspect ratios. In each case the extensional zone migrated outward with time as subsidence proceeded, small blocks breaking away and sliding into the depression (Figures 13 and 14). An important feature is that the width of the extensional zone is almost independent of roof aspect ratio (Figure 15). Thus at low aspect ratio the extensional zone is narrow compared with the entire width of the surface depression, whereas at high aspect ratios it dominates.

**7.3. Three-Dimensional Reservoir (Various Shapes)**

We carried out additional 3-D experiments to study the influence of reservoir shape on subsidence geometry. Silicone reservoirs were constructed with either flat roofs (three different shapes in plan view: square, rectangular, and elliptical; Figures 16 and 17) or rounded roofs (two different shapes: half cylinders

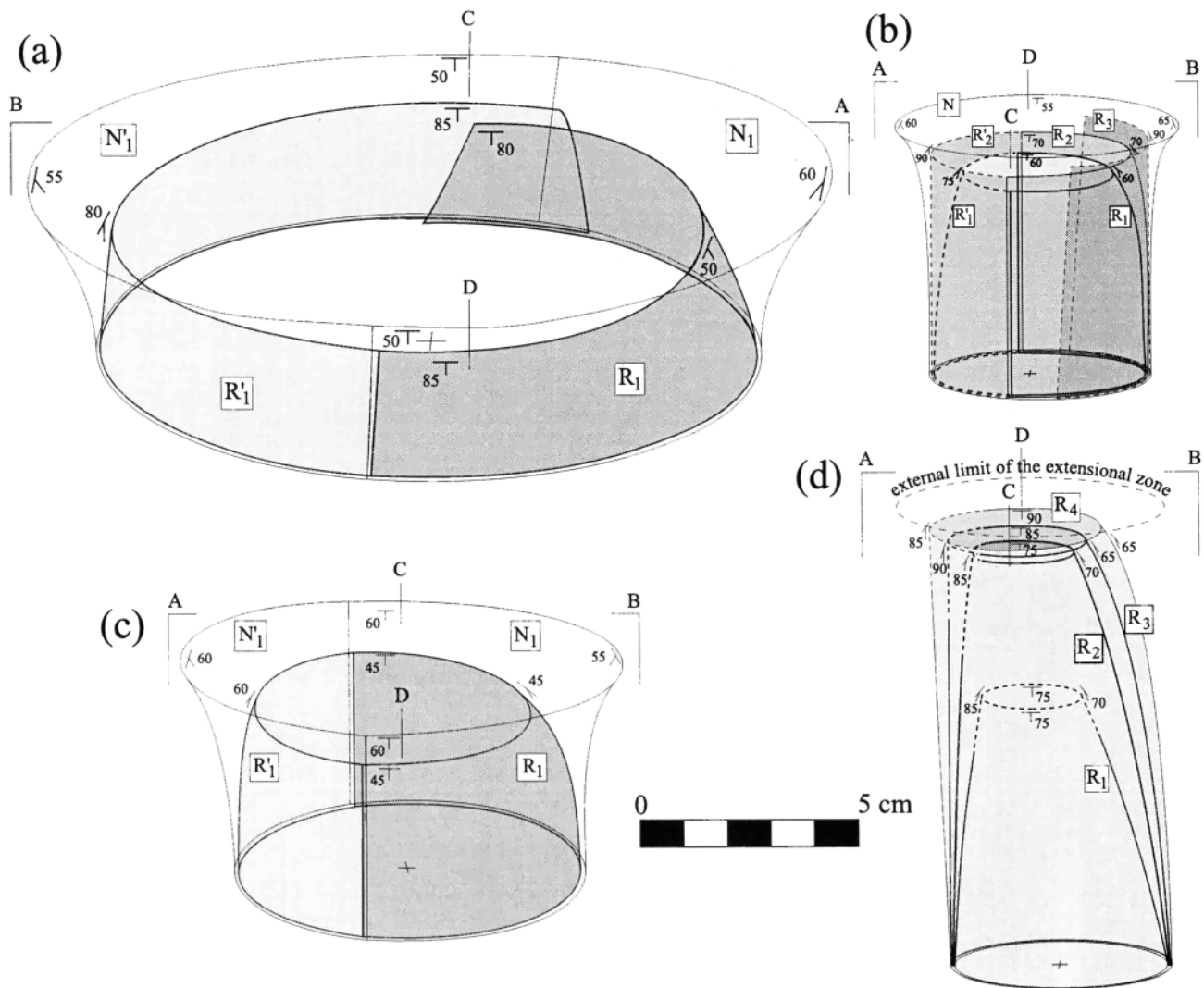


**Figure 10.** Diagrams summarising the structures of the 3-D experiments. Aspect ratios of (a) 0.2, (b) 1, (c) 0.5, and (d) 2. Reverse faults are marked R and normal faults N. Fault dips and lines of cross sections (AB; Figures 11 to 14) are indicated.

and half spheres, Figure 18). The aspect ratio of a rounded roof was defined using the minimum thickness. For each reservoir shape we investigated just two end-member roof aspect ratios (0.2 and 2).

Departure from a simple flat-roofed, cylindrical reservoir shape does not strongly influence the subsidence mechanism. However, the experiments revealed some interesting variations of fault geometry and propagation that might be relevant in nature.

Sharp corners (square, rectangle, half cylinder) acted to arrest propagating faults. Square and rectangular cases showed similar behavior. For a low roof aspect ratio a first reverse fault (numbered 1 on each of the figures) nucleated in the middle of one side and propagated sideways in each direction (Figures 16a and 16c). It was then arrested by the corners, and subsidence proceeded in a trapdoor fashion along one side of the reservoir. Subsequently, a second reverse fault (numbered 2) formed on the opposite side of the reservoir. The same was then repeated on the two other sides. The associated normal faults showed similar behavior.

The first reverse faults always nucleated along the long sides of an elongated reservoir (rectangle, ellipse, or half cylinder), irrespective of roof aspect ratio. For the elliptical reservoir a first reverse fault nucleated on one long side (numbered 1) followed by a second one on the opposite side. The two faults then propagated around and joined. Collapse into a reservoir with the shape of a half-cylinder produced a strongly asymmetric depression with a single large reverse fault parallel to the cylinder axis (Figure 18a). A notable feature of this experiment was that the dip of the sand layers increased progressively toward the depression axis.

Collapse commonly generated complicated accommodation structures in the marginal tilted blocks. In the square and rectangular cases the tilted block on the side of fault 1 was cut by multiple outward dipping normal faults (Figures 16a and 16c). For the half cylinder the tilted block was cut by multiple small normal faults, forming a graben. At low aspect ratios the surface depression had the same shape as the underlying reservoir, whereas this was less the case at high aspect ratios.

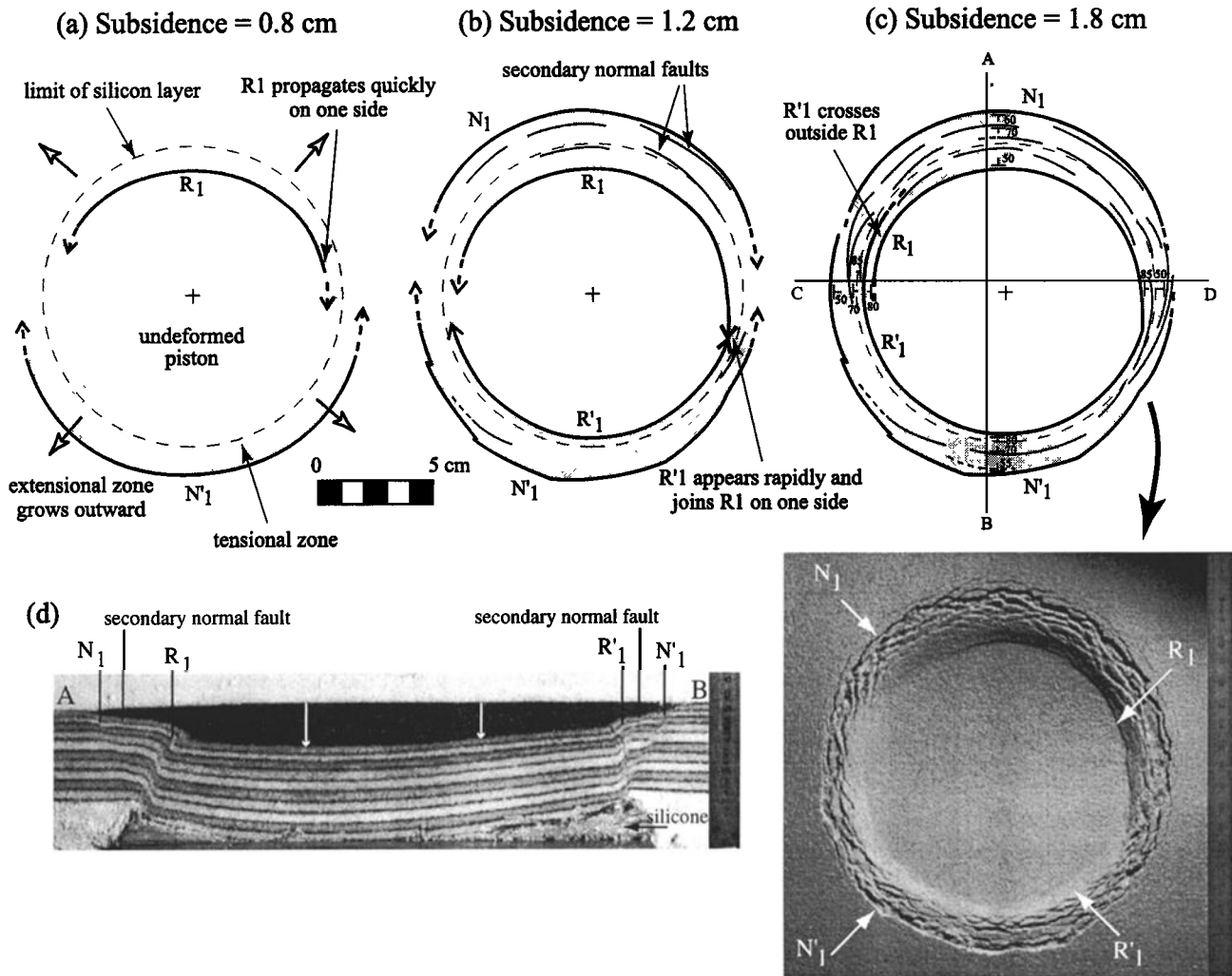


**Figure 11.** Three dimensional experiments. Roof aspect ratio of 0.2. (a-c) Temporal evolution of surface deformation in experiment 45. R, reverse fault; N, normal fault. The limit of the silicone layer at depth is shown. The extensional zone at the surface is shown shaded. The photograph shows the final structure at the surface: an extensional ring is delimited by reverse faults inside and normal faults outside. The external limit of the depression is a scarp a few millimeters high that corresponds to the intersection of the normal ring faults with the surface. (d) Cross section AB. The uppermost layer of black sand was placed on the model after the experiment to protect the collapse depression.

### 8. Stress Fields in the Experiments

Stress fields present in the experiments can be reconstructed qualitatively from the orientations and throws of observed faults (Figure 19). Numerical simulations of the experiments are being carried out to better constrain these patterns and will be reported elsewhere. In this paper we assume that the maximum shear stress  $\tau_{max}$  is vertical above the margins of the reservoir (Figure 20). According to theory [Jaeger and Cook, 1971; Price and Cosgrove, 1990], the angle between  $\tau_{max}$  and the principal normal stress  $\sigma_1$  is  $45^\circ$ . Furthermore, the angle  $\alpha$  between  $\sigma_1$  and the fault created is  $\alpha=45^\circ-\phi/2$ , where  $\phi$  is the angle of internal friction. In our case,  $\phi=34^\circ$ , so we obtain  $\alpha=28^\circ$ . This predicts that the first faults created should dip outward at  $73^\circ$  and agrees well with the dips ( $\sim 70^\circ$ ) of reverse faults generated in the experiments.

Given [1973] discusses the mechanism of subsidence above a rectangular mining cavity. The cavity induces a redistribution of the stress field above it. This produces an arch around which the lines of principal stress  $\sigma_1$  are deflected (Figure 21). Here  $\sigma_1$  beneath the arch is less than lithostatic (zone A, Figure 21). Outside the arch there is a zone in which  $\sigma_1$  exceeds lithostatic (zone B, Figure 21). The outer boundary of zone B is called the limit of influence. A deflected (vault-shaped) stress field serves to generate a maximum shear stress  $\tau_{max}$  near the cavity margins [e.g., Bamberger, 1997]. There is a competition between the vault effect, which tends to stabilize the edifice, and the shear stress, which disrupts it. Disruption of the cavity roof starts by formation of extensional fractures that coalesce and evolve into shear faults as they propagate upwards. These faults are reverse and dip outward.

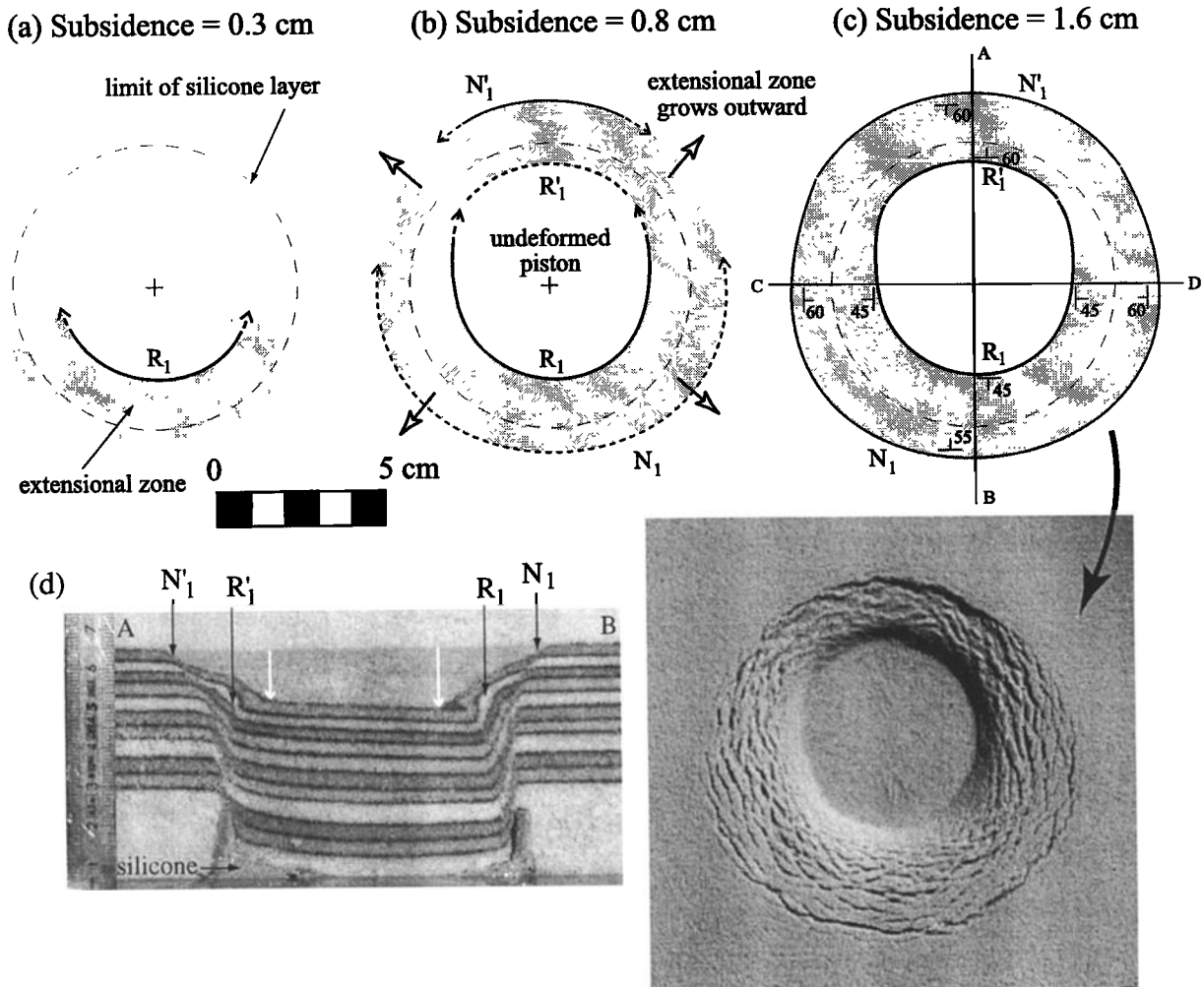


**Figure 12.** Three-dimensional experiments. Roof aspect ratio of 0.5. (a-c) Temporal evolution of surface deformation in experiment 36. R, reverse fault; N, normal fault. The limit of the silicone layer at depth is shown. The extensional zone at the surface is shown shaded. (d) Cross section AB. The uppermost layer of grey sand was placed on the model after the experiment to protect the collapse depression.

A vault-shaped stress field explains the structures produced at different roof aspect ratios in our experiments (Figure 19). At high roof aspect ratios the stress field generates a first set of reverse faults at depth that delimit a subsiding block. Stresses above this first block are then redistributed, and a second set of reverse faults forms. This process is repeated until the faults reach the surface. At low roof aspect ratios the lines of  $\sigma_1$  are still deflected but the arch intercepts the surface. Above the reservoir  $\sigma_1$  is close to lithostatic and the roof collapses as a coherent piston. Near the edge of the reservoir,  $\sigma_1$  induces formation of reverse faults, whereas farther out, being closer to vertical, it induces inward dipping normal faults.

The associations of vault-shaped principal stress fields, reverse faults, and normal faults are also known from studies of large-scale crustal motions. Examples include numerical modeling [Anderson, 1936; Hafner, 1951; Sanford, 1959; Couples, 1977; Gangi et al., 1977; Couples and Stearns, 1978], sand box experiments [Sanford, 1959; Horsfield, 1977; Vendeville, 1988], rock deformation under pressure [Friedman et al., 1976], and field studies [Couples and Stearns, 1978]. Previous experiments

on caldera collapse also revealed the formation of reverse outward dipping faults [Komuro, 1987; Martí et al., 1994].

## 9. Implications for Caldera Collapse and Ignimbrite Eruptions

We now consider the implications of our experiments for the collapse mechanisms of calderas. We highlight certain limitations of our experimental system. Owing to the granular nature of sand, it is impossible for silicone to inject in the manner of a ring dike. For this reason the experiments can only be considered truly representative of the natural system during the first stages of subsidence, before ring dikes form. The experiments are only applicable to calderas where there is no preliminary tumescence and no regional faults, or at least to examples where these features are not of major importance. In fact, evidence for major precollapse tumescence is elusive [Lipman, 1984]. Regional faults probably play an important role during collapse at many calderas [Walker, 1984]. In some cases, calderas collapse in a piecemeal fashion because the caldera block is broken up by

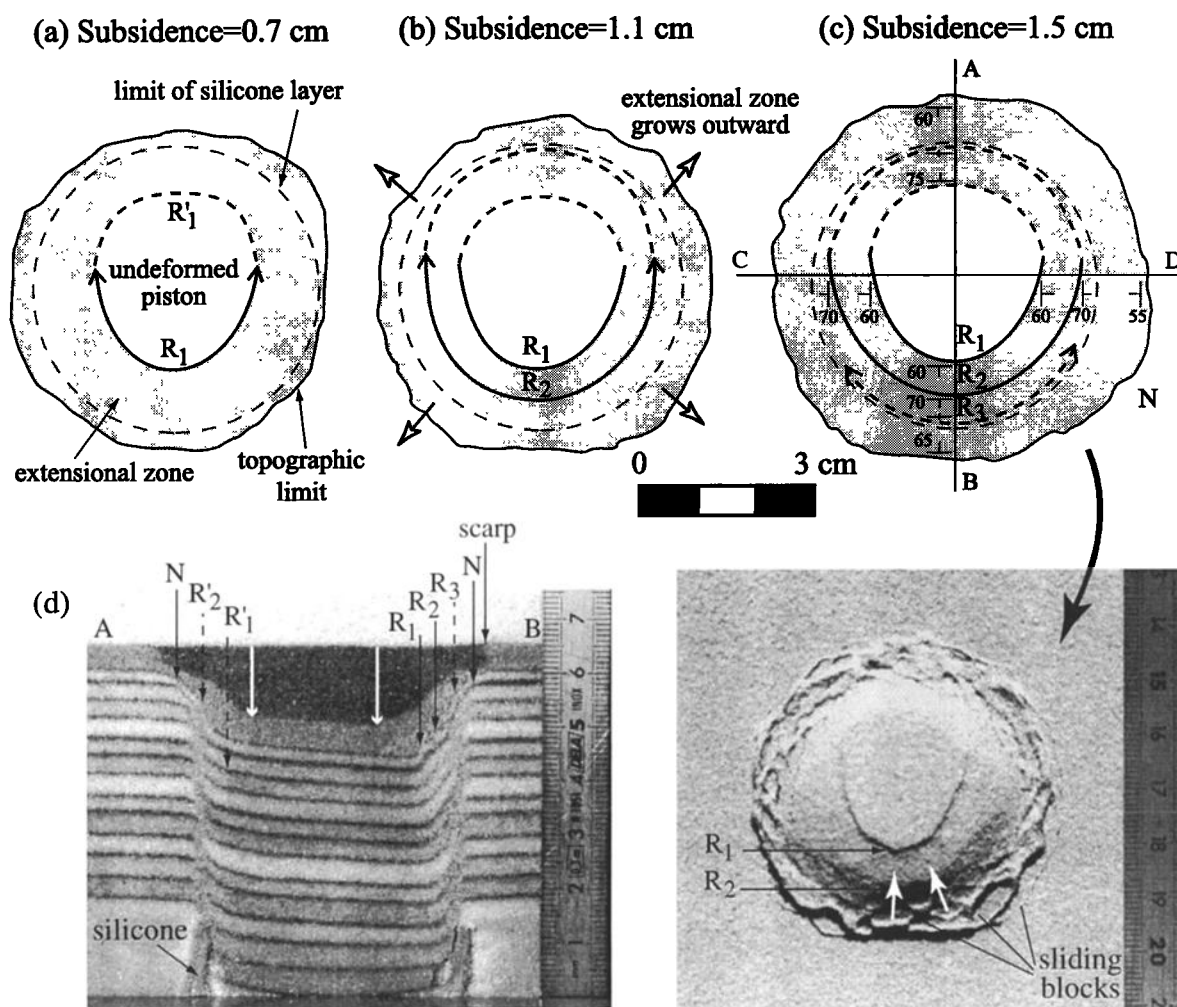


**Figure 13.** Three-dimensional experiments. Roof aspect ratio of 1. (a-c) Temporal evolution of surface deformation in experiment 38. R, reverse fault; N, normal fault. The limit of the silicone layer at depth is shown. The extensional zone at the surface is shown shaded. (d) Cross section AB. The uppermost layer of black sand was placed on the model after the experiment to protect the collapse depression.

networks of regional faults [Branney and Kokelaar, 1994; Moore and Kokelaar, 1997, 1998]. However, the circular or elliptical shapes of many large calderas and ring dike complexes show that the magma reservoir commonly dominates the stress field, as in our experiments. Some calderas may also be multicyclic, which further complicates their structural development. We neglect the role of regional faults and multicyclic in the following discussion, while acknowledging their significant role at many calderas.

The experiments revealed a general mechanism of subsidence into a flat-topped, cylindrical fluid-filled cavity. Collapse occurs principally along reverse or vertical faults, either as a coherent piston (low roof aspect ratio) or as a series of wedges or cones bounded by multiple faults (high roof aspect ratio). Variations on this theme are observed for more complex chamber shapes, but the essential mechanism is the same. An interesting feature of the experiments is that they generate (by a general subsidence mechanism) many structures observed in calderas and proposed in structural models (Figure 1). These include outward dipping reverse faults, vertical faults, inward dipping normal faults, roof

flexure, trapdoor (asymmetric) subsidence, coherent collapse, and a kind of noncoherent collapse in which the roof subsides as multiple large blocks. Depending on the exact cut through the final structure and on the amount of subsidence, some combination of these different features is always observed.

Once formed, reverse faults are predicted to play an important role in accommodating caldera subsidence, as also expected from space considerations. Many ring dikes in eroded calderas are observed to dip steeply outward [Richey, 1932; Oftedahl, 1978; Yoshida, 1984; John, 1995]. Seismic data at Rabaul caldera have revealed the existence of an elliptical, outward dipping ring fault [Mori and McKee, 1987; Jones and Stewart, 1997]. Another feature of the experiments is the occurrence of marginal zones of inward dipping strata and of updrag of strata along both normal and reverse faults. Inwardly inclined bedding and updrag against faults have been taken as evidence that the collapse of some calderas occurred mainly along inward dipping normal faults [Kingsley, 1931; Reynolds, 1956; Oftedahl, 1978; Yoshida, 1984]. However, our experiments generated these structures even though the main collapse faults were reverse and outward

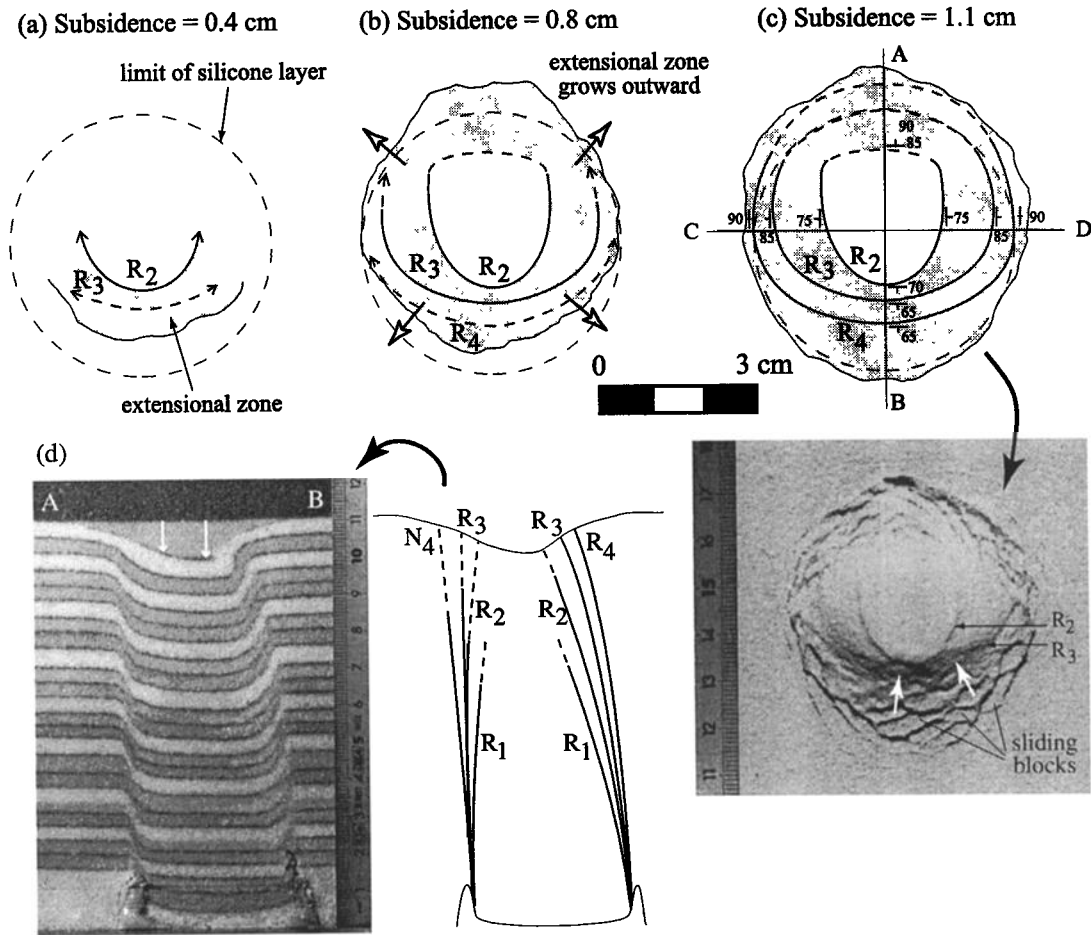
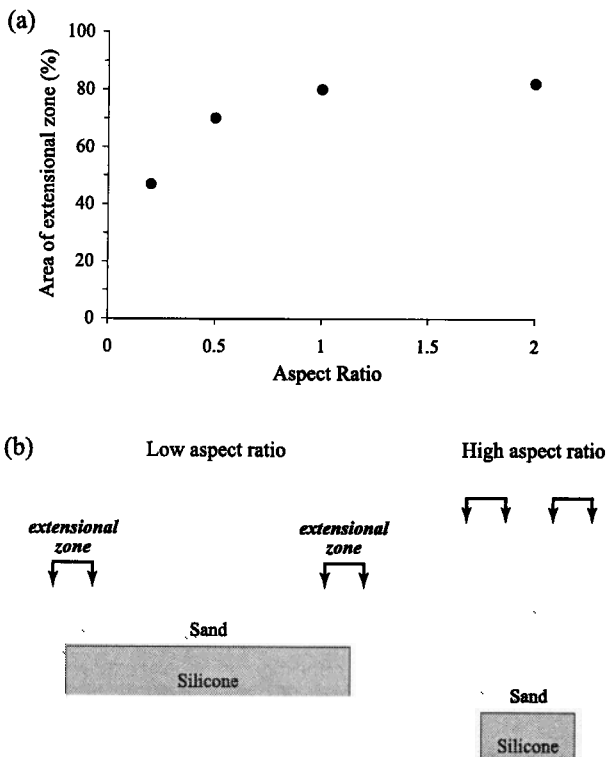


**Figure 14.** Three-dimensional experiments. Roof aspect ratio of 2. (a-c) Temporal evolution of surface deformation in experiment 43. R, reverse fault; N, normal fault. The limit of the silicone layer at depth is shown. The extensional zone at the surface is shown shaded. (d) Cross section AB. The uppermost layer of black sand was placed on the model after the experiment to protect the collapse depression.



dipping. The presence of inward dipping strata in calderas is not necessarily evidence for collapse uniquely along inwardly inclined ring faults, as also noted by *Branney* [1995], although normal faults are likely to be present and to play a role. We now discuss caldera collapse mechanisms using two end-member scenarios: a large, shallow magma chamber (low roof aspect ratio) and a small, deep magma chamber (high roof aspect ratio) (Figure 22).

**9.1. Large, Shallow Magma Chamber**

Collapse at low roof aspect ratios in the experiments commenced by flexural downsag of the roof, without formation of discrete faults. Deformation was taken up by intergranular slip distributed more or less homogeneously throughout the roof. This created a broad, shallow depression at the surface, with an annular zone of extension around the margins. Marginal flexure

**Figure 15.** (a) Percentage area of the collapse depression occupied by the annular extensional zone in the 3-D experiments with cylindrical reservoir. (b) The width of the extensional zone is almost constant between experiments. At low roof aspect ratios the extensional zone is relatively thin compared to the diameter of the whole depression. At high roof aspect ratio it dominates the depression.

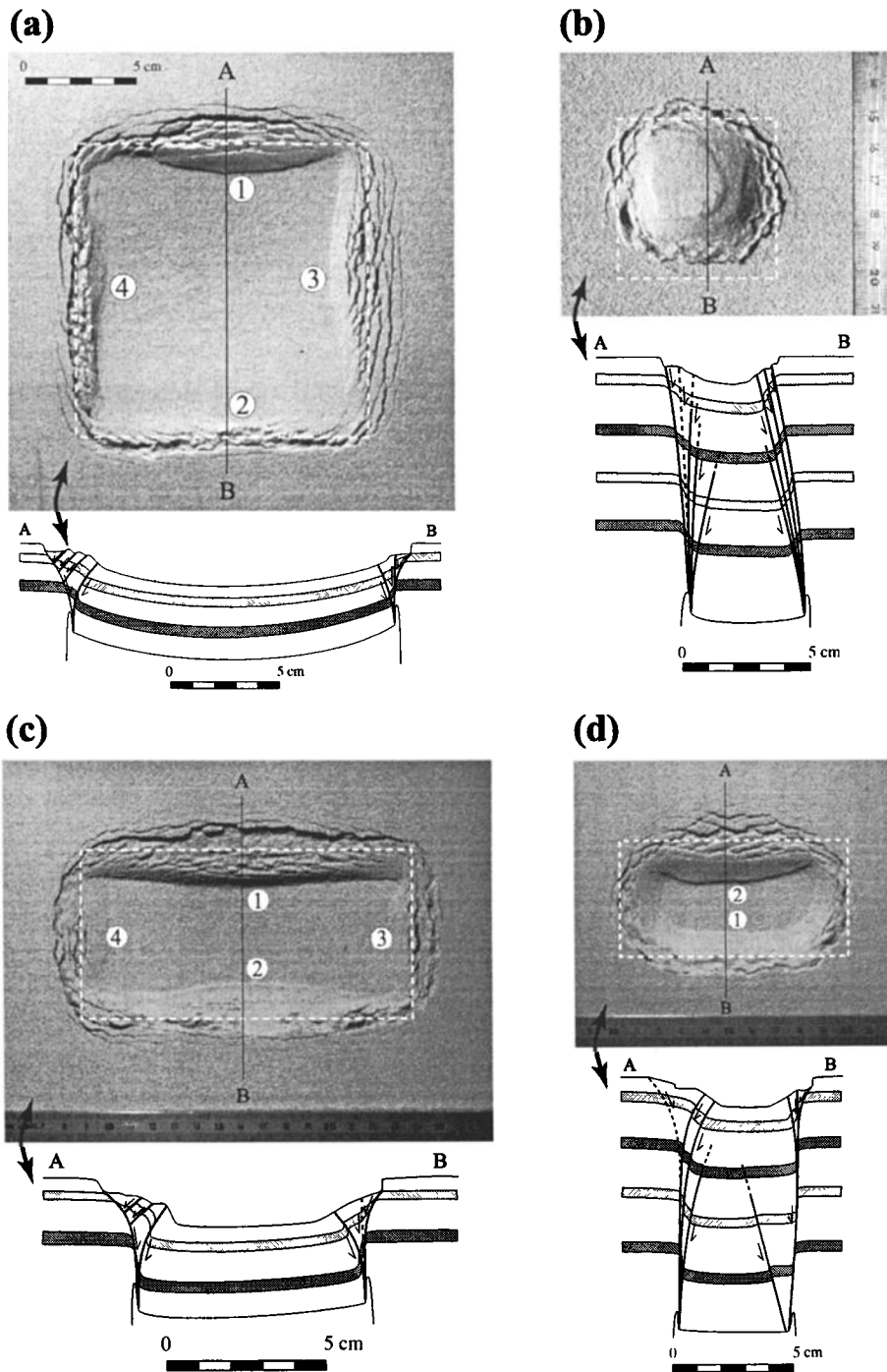


**Figure 16.** Three-dimensional experiments. Silicone reservoirs with flat roofs and square (Figures 16a and 16b) or rectangular (Figures 16c and 16d) shapes in plan view. The limit of the silicone layer at depth is shown (thin dashed line). (a) Experiment 47, roof aspect ratio 0.2; (b) experiment 48, aspect ratio 2; (c) experiment 49, aspect ratio 0.2; and (d) experiment 50, aspect ratio 2. Numbers indicate the order of fault nucleation.

also continued to occur after the first faults appeared at depth. Flexural downsag has been proposed for some relatively small-volume eruptions [Branney, 1995] and might be expected for some calderas with low subsidence/diameter ratios or during the initial stages of large collapses. In such cases the deformation might be distributed over a large number of small faults in the subsiding block. Significant downsag would also be favored by a mechanically weak crust, a strong crust favoring the onset of

large-scale faulting at an early stage in the subsidence. Some calderas such as Bolsena and Taupo [Walker, 1984] have been interpreted as purely downsag. Examples of faulted calderas with a significant downsag component include Tavua [Setterfield *et al.*, 1991] and Glen Coe [Moore and Kokelaar, 1997, 1998]. Walker [1984] and Branney [1995] have speculated that downsag could represent half the total subsidence in some calderas.

Our experiments suggest that in the absence of extant faults

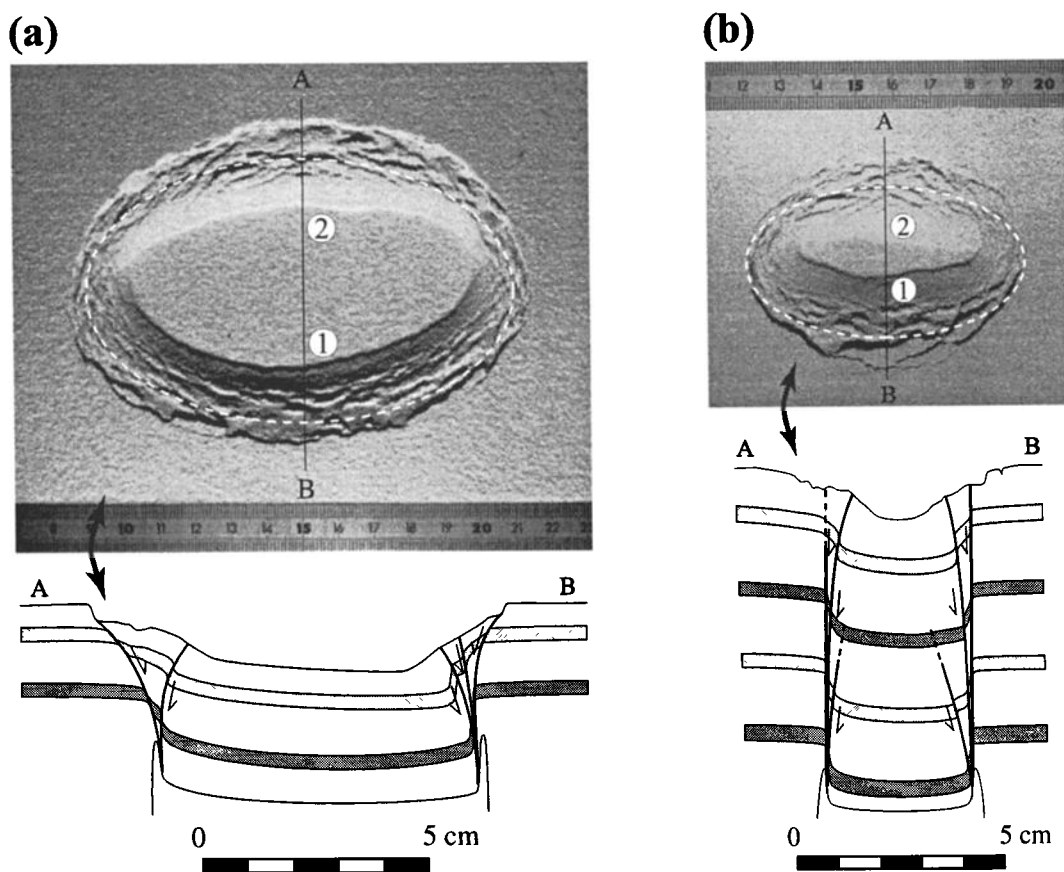


**Figure 17.** Three-dimensional experiments. Silicone reservoir with flat roof and elliptical shape in plan view (long axis twice that of small). The limit of the silicone layer at depth is shown (thin dashed line). (a) Experiment 53, roof aspect ratio 0.2, and (b) experiment 59, aspect ratio 2. Numbers indicate the order of fault nucleation.

and other crustal heterogeneities, the first major faults generated during caldera collapse should be reverse with outward dips. This is in agreement with simple collapse theory [Anderson, 1936]. Collapse in many of the experiments occurred in an asymmetric, or trapdoor, fashion, as commonly observed in calderas. In cases of low roof aspect ratio, significant displacement on the first reverse fault occurred before nucleation of the second on the opposite side of the reservoir. Previously suggested causes of trapdoor collapse include the existence of an asymmetric chamber [Lipman, 1997] and preferred magma withdrawal from one side of the caldera [Varga and Smith, 1984]. The experiments show that the degree of asymmetry of the chamber or roof need not be very great for trapdoor collapse to occur. Collapse initiates preferentially on the side of the caldera where the roof thickness is greatest. In many experiments the initial collapse was asymmetric but became more symmetric later on once the reverse faults had propagated completely around the reservoir. Other factors favoring trapdoor collapse might be injection of magma (and consequent friction reduction) along early formed faults and the ponding of intracaldera ignimbrite in the asymmetric depression.

As a caldera subsides, support is removed from the surrounding rocks. This generates an annular zone of flexure and extension in which strata are rotated down and into the depression [Branney, 1995]. Complex accommodation structures can form in this zone, including multiple outward dipping reverse

faults, outward dipping normal faults, and grabens (Figures 9, 16a, 16c, and 18a). An interesting comparison can be made between the experiments and some large U.S. calderas. At many calderas of the San Juan Mountains the main ring faults (marked by a ring of postcaldera domes) have diameters in the range 10 to 15 km, whereas those of the topographic rims are 13 to 20 km [Lipman, 1976, 1984] (Figure 23). The topographic rim lies up to 5 km outboard of the main collapse faults. Lipman [1976] interpreted the intervening zone as the source of the landslide megabreccias found in intracaldera ignimbrites. The scaled width of the landslide zone in a typical San Juan caldera is about the same as that of the annular extensional zone in our 0.2 aspect ratio experiments. We speculate that the topographic rims of many large calderas coincide approximately with the outer limit of the extensional zone. An inward dipping normal ring fault may, or may not, be present outboard of the extensional zone, depending on the caldera dimensions, subsidence depth and rock properties.

## 9.2. Small, Deep Magma Chamber

The collapse mechanism is somewhat different at roof aspect ratios greater than  $\sim 1.5$ . The initial reverse faults no longer reach the surface but intersect at depth, triggering formation of other faults at higher levels. These multiple faults slice the subsiding block up into a series of wedges or cones, and the block no

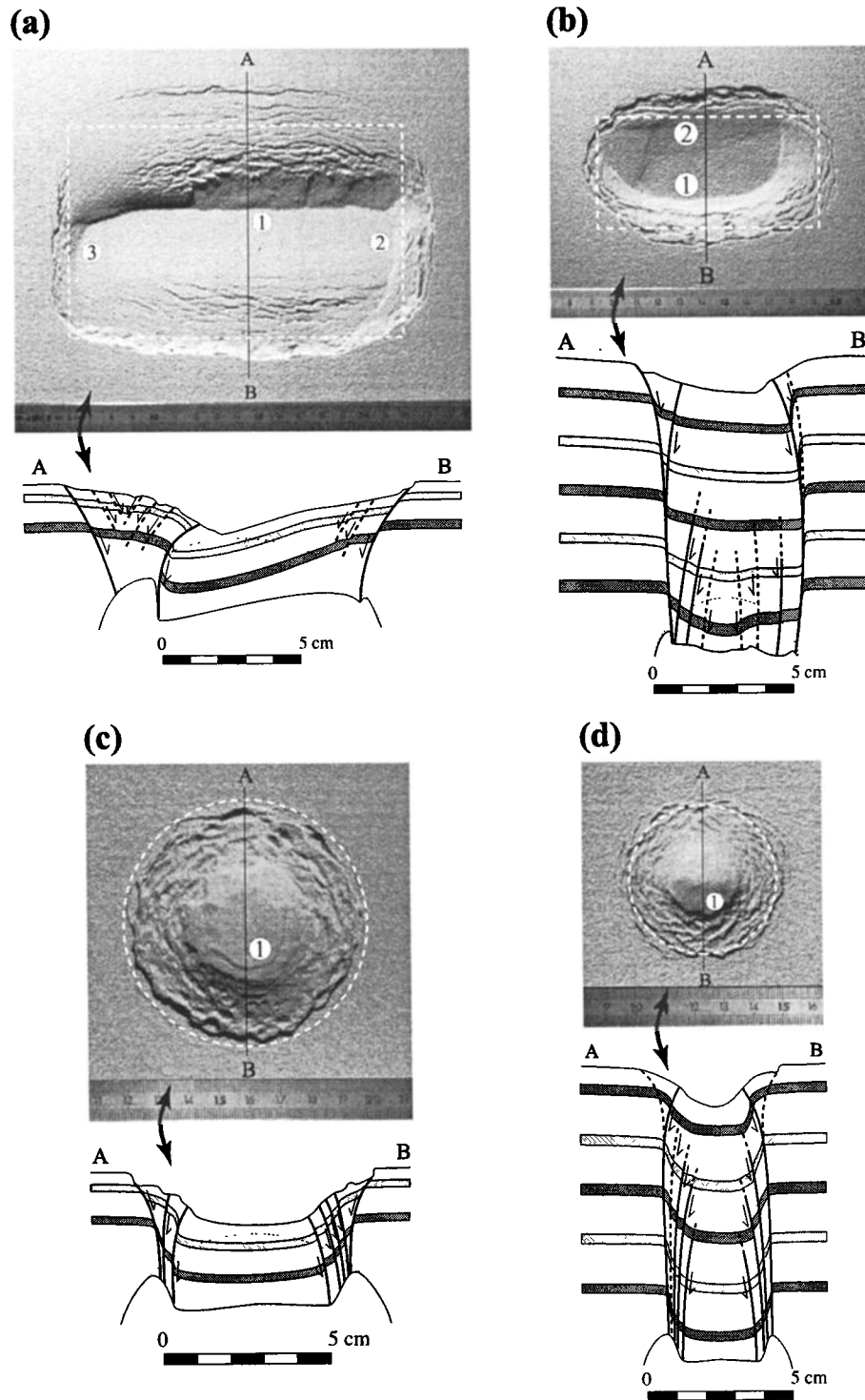


**Figure 18.** Three-dimensional experiments. Silicone reservoir with the shapes of a half-cylinder (Figures 18a and 18b) (length/width of 1.6 to 2) and a half-sphere (Figures 18c and 18d). The limit of the silicone layer at depth is shown (thin dashed line). (a) Experiment 52, roof aspect ratio 0.2, (b) experiment 51, aspect ratio 2, (c) experiment 57, aspect ratio 0.2, and (d) experiment 56, aspect ratio 2. Numbers indicate the order of fault nucleation.

longer collapses as a coherent entity. In reality, intrusion of magma along these faults would result in the stoping of multiple large blocks into the chamber, without the formation of a single, well-defined ring dike. In fact, there is a marked lack of ring dikes less than ~10 km across [Walker, 1984]. This is about the

minimum caldera size expected for coherent collapse, given a typical magma chamber depth of several kilometers.

Another feature of collapse at high roof aspect ratio is that the annular extensional zone dominates the depression. The width of this zone is only a weak function of roof aspect ratio, so that at

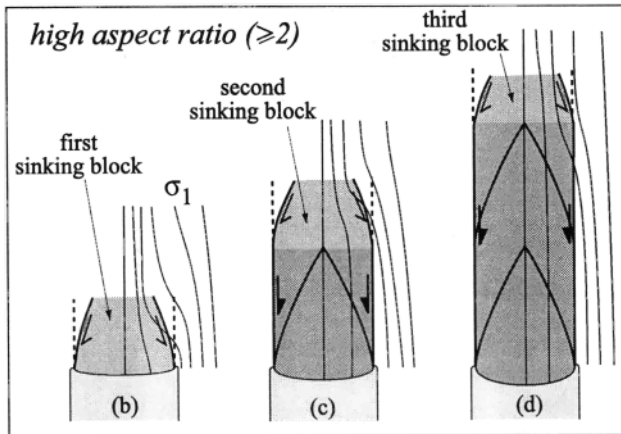
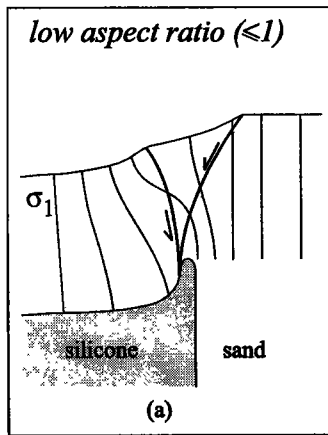


**Figure 19.** Schematic representation of the principal stress fields ( $\sigma_1$ ) reconstructed qualitatively from fault patterns observed in the experiments. See the text for discussion.

ratios greater than  $\sim 1$  it would account for at least 80% of the caldera depression (Figure 15). This is in broad agreement with the critical aspect ratio of 0.7 predicted by mining subsidence models (Figure 2). We now discuss the implications of this for the origin of funnel calderas.

**9.3. Funnel Calderas**

Several different origins have been proposed for funnel calderas. It has been suggested that they are essentially large breccia-filled explosion craters, reamed out during eruption [Yokoyama, 1981, 1992; Yokoyama and Mena, 1991]. However, the volume of lithic fragments in many ignimbrites is too low to account for the caldera depression [Self and Rampino, 1981]. Neither is the energy available during explosive eruptions sufficient to create very large explosion craters [Scandone, 1990]. By analogy with nuclear cavities, Scandone [1990] proposed that funnel calderas form by chaotic collapse and that this would explain their characteristic U-shaped gravity anomalies. Another factor might be the nature of the crust. Walker [1984] suggested that funnel calderas form preferentially on young, hot (and weak) crust, such as island arcs. However, piston calderas with well-defined ring faults such as Kakeya [Sawada, 1984], Ischizuki [Yoshida, 1984], Kasagata [Harayama, 1992], and Tamagawa [Suto, 1992] are known from the Japanese arc. It has also been suggested that tectonic regime plays a role, funnel and piston

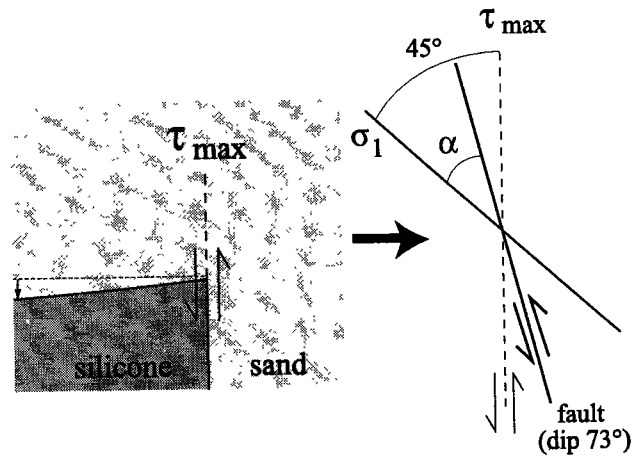


**Figure 20.** Mechanical model showing the maximum vertical shear stress and the resulting vault-shaped stress field above the margins of the silicone reservoir. The first fault created is reverse and dips outward at a theoretical angle of  $\alpha=73^\circ$ . See the text for discussion.

calderas forming in compressive and extensive environments respectively [Sawada, 1984; Yoshida, 1984]. However, this does not appear to be valid because some funnel calderas such as Shishimuta form in extensional regimes [Kamata, 1989, 1992].

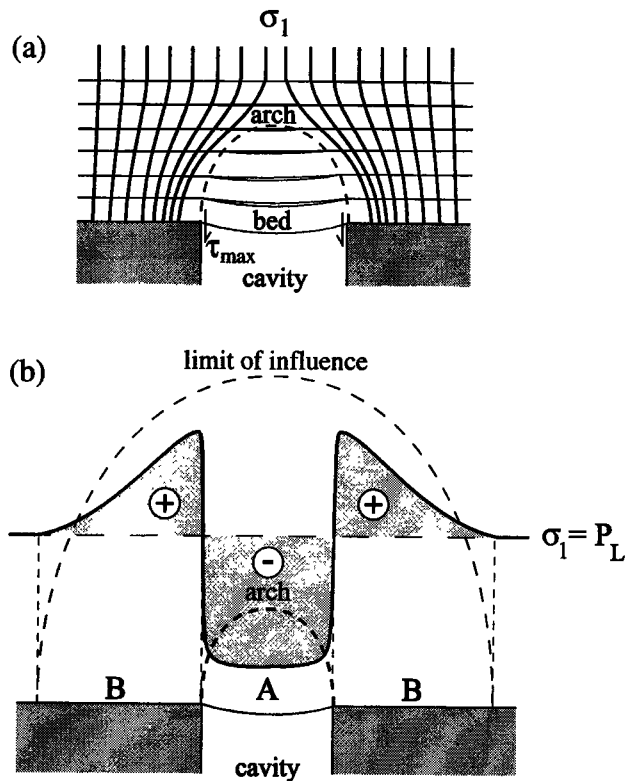


**Figure 21.** (a) Stress field above a rectangular cavity in a mine (high roof aspect ratio). The presence of the cavity serves to deflect the lines of the principal stress  $\sigma_1$  around an arch-shaped zone. The horizontal lines represent strata. (b) The  $\sigma_1$  under the arch is less than the lithostatic stress,  $P_L$  (zone A). Outside the arch there is a zone B in which  $\sigma_1$  exceeds lithostatic. The outer limit of zone B is called the limit of influence. The lateral variation of  $\sigma_1$  at the level of the top of the cavity is shown. Modified from Vidal [1961] and Given [1973].

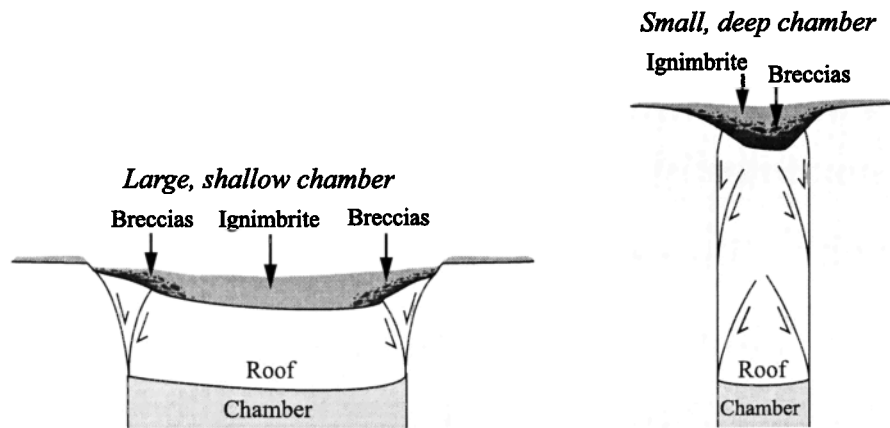


**Figure 22.** Schematic representation of two end-member caldera types based on the laboratory experiments. The case of a small, deep chamber might relate to some funnel calderas.

Hallinan [1993] and Hallinan and Brown [1995] attributed the funnel shape to multiple subsidence, triggering the formation of ring faults of decreasing diameter.

Our experiments provide an alternative explanation of some funnel calderas. A similar origin has been proposed recently by Lipman [1997] based on field observations and geometric arguments. We suggest that some funnel calderas are the surface manifestations of collapse into relatively small, deep magma chambers by disruption of the roof and the stoping of large blocks. They would as such correspond to the high aspect ratio end-member proposed in Figure 22. A feature of many funnel calderas is indeed their small diameter. In such calderas the extensional zone is likely to dominate the surface depression, and any coherent piston would be small or absent. Surface extension during collapse would favor mass wasting from the margins of

the caldera toward the center in the form of landslides. The collapse of such calderas is likely to generate a V- or U-shaped depression, as in the experiments (Figures 14, 16, 17, and 18), with landslide megabreccias accounting for a large fraction of the caldera fill. Quantities of lithic breccia and slide lenses are indeed observed by drilling in funnel calderas [Kurozumi and Doi, 1994, 1995; Ando et al., 1992; Awata, 1992]. This mechanism for the origin of some funnel calderas is appealing because the essential collapse mechanics is the same as for piston calderas. In this interpretation, funnel calderas are simply one end-member of a spectrum of collapse structures produced by the same physical processes. Since the origin is one of collapse, there is no need for large volumes of ejected lithics, as in the remaining origin. Our experiments are consistent with a gradation of collapse processes and structures from large piston calderas to funnel calderas

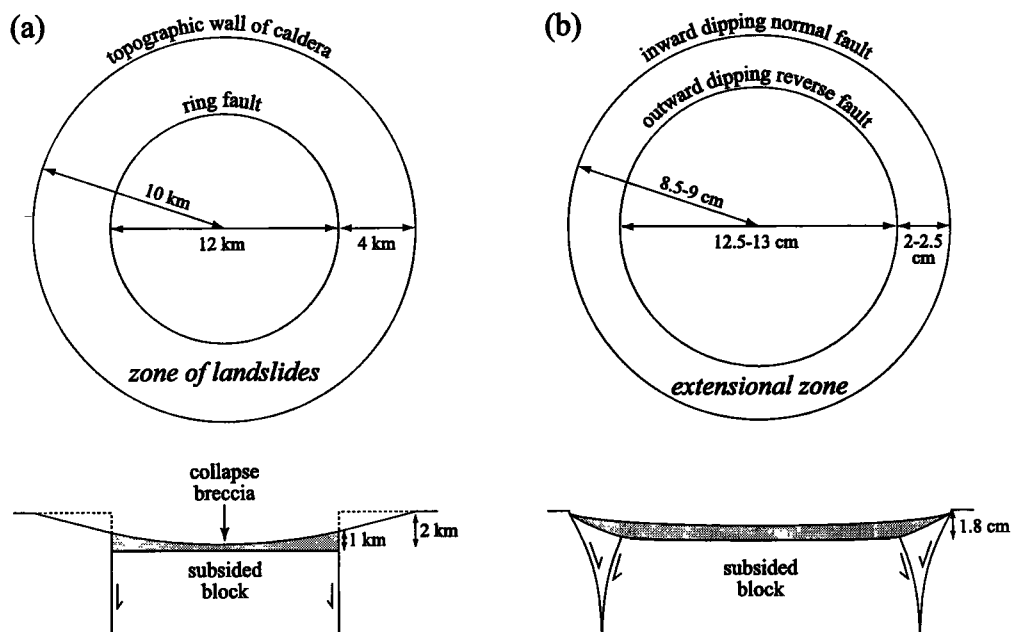


**Figure 23.** (a) Structural model for calderas of the San Juan Mountains, based on Lipman [1976]. (b) An alternative interpretation, based on the laboratory experiments, in which the annular extensional zone acts as the source for landslides. The inward dipping normal ring fault outboard of the extensional zone may not always be present in nature.

[Lipman, 1997]. We stress that some small calderas with very lithic-rich ejecta may owe their origin to a significant component of explosive reaming. Particularly small so-called funnel calderas, such as Nigorikawa (3 km across) are perhaps best interpreted as large vents.

#### 9.4. Implications for Vent Evolution During Ignimbrite Eruptions

Spatial and temporal evolution of syncollapse fault networks exerts a strong influence on the style, intensity, and duration of caldera-forming ignimbrite eruptions. During large explosive eruptions the chamber pressure decreases as magma vesiculates and fragments and is discharged at the surface [Druitt and Sparks, 1984; Bower and Woods, 1998]. Once the chamber is sufficiently underpressured, the roof is no longer supported and begins to subside. In the case of small, deep chambers, there may be a transition from an initial central vent to multiple vents as the roof breaks up and sinks as large blocks into the magma. In other cases, collapse may occur along regional faults, with linear vents opening up as the faults are activated [Heiken and McCoy, 1984].

At large, shallow chambers where regional faults play a less important role, vent evolution is likely to be related to the nucleation and propagation of ring faults. Magma will erupt preferentially where reverse ring faults dip outward and thus open during collapse. Inward dipping ring faults will not act as efficient conduits, since the magma must remain sufficiently overpressured to keep them open throughout the eruption. The experiments suggest that during collapse into large, shallow chambers, vents might open up on opposite sides of the magma chamber, then propagate around the caldera as it unzips. At elliptical calderas the vents are expected to first appear along the long edges of the caldera. Recent analysis of vent evolution during the 0.76 Ma Bishop Tuff eruption has revealed a pattern of vent development that agrees well with these predictions [Hildreth and Mahood, 1986; Wilson and Hildreth, 1997]. The first vent(s) appeared on the southern rim of the E-W elongated Long Valley caldera, then migrated about 90° anticlockwise around the ring fault. At the same time a complementary series of vents opened from west to east along the northern rim. Vents at trapdoor calderas are expected to be concentrated along the edge of maximum subsidence, as at Snowdon [Howells et al., 1986]. Significant departures from these predictions are expected in many caldera systems due to variations in chamber geometry, regional stress patterns, and crustal heterogeneities.

**Acknowledgments.** Charles Carrigan, Peter Lipman, Steve Sparks, and an anonymous reviewer provided helpful reviews. Financial support was provided by the Observatoire de Physique du Globe de Clermont-Ferrand and by the Centre de Recherches Volcanologiques.

#### References

- Anderson, E.M., The dynamics of the formation of cone-sheets, ring dykes and caldron subsidences, *Proc. R. Soc. Edinburgh*, 56, 128-157, 1936.
- Ando, S., T. Kurozumi, and R. Komatsu, Structure and caldera fill deposits of Nigorikawa caldera, paper presented at 29th International Geological Congress, Kyoto, Japan, 1992.
- Aramaki, S., Formation of the Aira caldera, southern Kyushu, ≈22000 years ago, *J. Geophys. Res.*, 89(B10), 8485-8501, 1984.
- Aramaki, S., Underground structures of the Japanese late Pleistocene calderas are mostly funnel-shaped, paper presented at 29th International Geological Congress, Kyoto, Japan, 1992.
- Awata, Y., Internal geology and eruptive development of the Kawafune caldera, Japan, paper presented at 29th International Geological Congress, Kyoto, Japan, 1992.
- Bacon, C., Eruptive history of Mount Mazama and Crater Lake caldera, Cascade range, USA, *J. Volcanol. Geotherm. Res.*, 18, 57-115, 1983.
- Bamberger, Y., *Mécanique de l'Ingénieur, vol. III, Solides Déformables*, 452 pp., Hermann, Paris, 1997.
- Bower, S.M., and A.W. Woods, On the influence of magma chambers in controlling the evolution of explosive volcanic eruptions, *J. Volcanol. Geotherm. Res.*, 86, 67-78, 1998.
- Branney, J.M., Downsag and extension at calderas. New perspectives on collapse geometries from ice-melt, mining, and volcanic subsidence, *Bull. Volcanol.*, 57, 303-318, 1995.
- Branney, M.J., and P. Kokelaar, Volcanotectonic faulting, soft state deformation, and rheomorphism of tuffs during development of a piecemeal caldera, English Lake District, *Geol. Soc. Am. Bull.*, 106, 507-530, 1994.
- Clough, C.T., H.B. Maufe, and E.R. Bailey, The cauldron subsidence of Glen-Coe and the associated igneous phenomena, *Q. J. Geol. Soc. London*, 65, 611-678, 1909.
- Couples, G., Stress and shear fracture (fault) patterns resulting from a suite of complicated boundary conditions with applications to the Wind River Mountains, *Pure Appl. Geophys.*, 115, 113-133, 1977.
- Couples, G., and D.W. Stearns, Analytical solutions applied to structures of the Rocky Mountains foreland on local and regional scale, *Mem. Geol. Soc. Am.*, 151, 313-335, 1978.
- Druitt, T.H., and R.S.J. Sparks, On the formation of calderas during ignimbrite eruptions, *Nature*, 310, 679-681, 1984.
- Duran, J., *Sables, Poudres et Grains: Introduction à la Physique des Milieux Granulaires*, 251 pp., Eyrolles Sci., Paris, 1997.
- Elston, W.E., Mid-Tertiary ash flow tuffs cauldrons, southwestern New Mexico, *J. Geophys. Res.*, 89(B10), 8733-8750, 1984.
- Elston, W.E., and G.S. Plumlee, A special issue on volcanic centres as targets for mineral exploration: Preface, *Econ. Geol.*, 89(8), 1661, 1994.
- Fiske, R.S., and O.T. Tobisch, Middle Cretaceous ash-flow tuff and caldera collapse deposit in the Minarets caldera, east-central Sierra Nevada, California, *Geol. Soc. Am. Bull.*, 106, 582-593, 1994.
- Fridrich, C.J., R.P. Smith, E.D. DeWitt, and E.H. McKee, Structural, eruptive, and intrusive evolution of the Grizzly Peak caldera, Sawatch Range, Colorado, *Geol. Soc. Am. Bull.*, 103, 1160-1177, 1991.
- Friedman, M., J. Handin, J.M. Lagon, K.D. Min, and D.W. Stearns, Experimental folding of rocks under confining pressure, part III, Faulted drape folds in multilithologic layered specimens, *Geol. Soc. Am. Bull.*, 97, 1049-1066, 1976.
- Gangi, A.F., K.D. Min, and J.M. Logan, Experimental folding of rocks under confining pressure, part IV, Theoretical analysis of faulted drape folds, *Tectonophysics*, 42, 227-260, 1977.
- Geist, D., K.A. Howard, A.M. Jellinek, and S. Rayder, The volcanic history of volcan Alcedo, Galapagos archipelago. A case study of a rhyolitic oceanic volcanism, *Bull. Volcanol.*, 56, 243-260, 1994.
- Given, I.A. (Ed.), *Mining Engineering Handbook*, Part City Press, New York, 1973.
- Goff, F., and J.N. Gardner, Valles caldera region, New Mexico, and the emerging Continental Scientific Drilling Program, *J. Geophys. Res.*, 93(B6), 5997-5999, 1988.
- Gudmundsson, A., Formation of collapse calderas, *Geology*, 16, 808-810, 1988.
- Gudmundsson, A., J. Martí, and E. Turon, Stress field generating ring faults in volcanoes, *Geophys. Res. Lett.*, 24(13), 1559-1562, 1997.
- Hafner, W., Stress distributions and faulting, *Geol. Soc. Am. Bull.*, 62, 373-398, 1951.
- Hallinan, S., Non chaotic collapse at funnel caldera: Gravity study of the ring fractures of the Guayabo caldera, Costa Rica, *Geology*, 21, 367-370, 1993.
- Hallinan, S., and G. Brown, Incremental collapse and stratocone growth within a funnel shape calderas, Guayabo, Costa Rica, *J. Volcanol. Geotherm. Res.*, 67, 101-122, 1995.
- Handin, J., Handbook of physical constants. Strength and ductility, *Mem. Geol. Soc. Am.*, 97, 223-289, 1966.
- Harayama, S., Structure and collapse timing of deeply dissected calderas in the Japan Alps, paper presented at 29th International Geological Congress, Kyoto, Japan, 1992.
- Heiken, G., and F. Goff, Hot dry rock geothermal energy in the Jemez volcanic field, New Mexico, *J. Volcanol. Geotherm. Res.*, 15, 223-246, 1983.
- Heiken, G., and F. McCoy Jr., Caldera development during the Minoan eruption, Thira, Cyclades, Greece, *J. Geophys. Res.*, 89(B10), 8441-8462, 1984.
- Heiken, G., F. Goff, J.N. Gardner, W.S. Baldrige, J.B. Hulén, D.N.

- Nielson, and D Vaniman, The Valles/Toledo caldera complex, Jemez Volcanic Field, New Mexico, *Ann. Rev. Earth Planet Sci.*, 18, 27-53, 1990.
- Hildebrand, R S , Folded cauldron of the early Proterozoic Labine Group, northwestern Canadian Shield, *J. Geophys. Res.*, 89(B10), 8429-8440, 1984.
- Hildreth, W., Kulshan caldera: A Quaternary subglacial caldera in the North Cascades, Washington, *Geol. Soc. Am. Bull.*, 108, 786-793, 1996.
- Hildreth, W., and G.A. Mahood, Ring fracture eruption of the Bishop tuff, *Geol. Soc. Am. Bull.*, 97, 396-403, 1986.
- Hoek, E., P.K. Kaiser, and W.F. Bawden, *Support of Underground Excavation in Hard Rock*, 215 pp., A.A Balkema, Rotterdam, Netherlands, 1995.
- Horsfield, W T , An experimental approach to basement control faulting, *Geol. Mijnbouw*, 56(4), 363-370, 1977.
- Howells, M.F., A.J. Reedman, and D.G. Campbell, The submarine eruption and emplacement of the lower rhyolitic tuff formation (Ordovician), N Wales, *J. Geol. Soc. London*, 143, 411-423, 1986.
- Hubbert, M.K., Theory of scale models as applied to the study of geologic structures, *of the Geol. Soc. Am. Bull.*, 48, 1459-1520, 1937
- Hubbert, M.K., Mechanical basis for certain familiar geologic structures, *Geol. Soc. Am. Bull.*, 62, 355-372, 1951.
- Jaeger, J.C., and N.G.W Cook, *Fundamentals of Rock Mechanics*, 585 pp., Chapman and Hall, New York, 1971.
- John, D.A., Tilted middle Tertiary ash-flow calderas and subjacent granitic plutons, southern Stillwater Range, Nevada: Cross section of an Oligocene igneous centre, *Geol. Soc. Am. Bull.*, 107, 180-200, 1995.
- Jones, R.H., and R.C. Stewart, A method for determining significant structures in a cloud of earthquakes, *J. Geophys. Res.*, 102(B4), 8245-8254, 1997.
- Kamata, H., Shishimuta caldera, the buried zone of the Yabakei pyroclastic flow in the Hoho volcanic zone, Japan, *Bull. Volcanol.*, 51, 41-50, 1989.
- Kamata, H., Subsurface structure and tectonic setting of Shishimuta caldera, a funnel-shaped caldera in central Kyushu, Japan, paper presented at 29th International Geological Congress, Kyoto, Japan, 1992.
- Kingsley, L., Cauldron subsidence of the Ossipee Mountains, *Am. J. Sci.*, 22, 139-168, 1931.
- Komuro, H., Experiments on cauldrons formation: A polygonal cauldron and ring fractures, *J. Volcanol. Geotherm. Res.*, 31, 139-149, 1987.
- Komuro, H., Y. Fujita, and K. Kodama, Numerical and experimental models on the formation mechanism of collapse basins during the Green Tuff orogenesis of Japan, *Bull. Volcanol.*, 47, 649-666, 1984.
- Kuno, H., Y. Oki, K. Ogino, and S. Hirota, Structure of Hakone caldera as revealed by drilling, *Bull. Volcanol.*, 31, 713-725, 1971.
- Kurozumi, H., and N. Doi, Inner structure of the Nigorikawa caldera, part 2, paper presented at Fall Meeting, Volcanol. Soc of Japan. Kyushu Univ., Fukuoka, Japan, 1994
- Kurozumi, H., and N. Doi, Inner structure of the funnel-shaped Nigorikawa caldera clarified by 3 km deep geothermal wells, Hokkaido, Japan, paper presented at IUGG XXI General Assembly, Univ. Of Colo., Boulder, 1995.
- Lipman, P.W., Evolution of the Platoro caldera complex and related volcanic rocks, south-eastern San Juan mountains, Colorado, *U.S. Geol. Surv. Prof. Pap.*, 852, 128 pp., 1975.
- Lipman, P.W., Caldera collapse breccia in the western San Juan Mountains, Colorado, *Geol. Soc. Am. Bull.*, 87, 1397-1410, 1976.
- Lipman, P.W., The Miocene Questa caldera, northern New Mexico: Relation to batholith emplacement and associated molybdenum mineralization, in *The genesis of Rocky Mountains Ore Deposits: Changes With Time and Tectonics, Symp. 1983*, vol.1, pp. 133-148, Denver Reg. Explor. Geol. Soc., Lakewood, Colo, 1983
- Lipman, P.W., The roots of ash flow calderas in the western North America: windows into the tops of granitic batholiths, *J. Geophys. Res.*, 89(B10), 8801-8841, 1984.
- Lipman, P.W., Subsidence of ash-flow calderas: Relation to caldera size and magma chamber geometry, *Bull. Volcanol.*, 59, 198-218, 1997.
- Lipman, P.W., O.A. Bogatkov, A.A. Tsvetkov, C. Gazis, A.G. Gurbanov, K. Hon, N.V. Koronovsky, V.I. Kovalenko, and P. Marchev, 2.8-Ma ash-flow caldera at Chegem River in the northern Caucasus Mountains (Russia), contemporaneous granites, and associated ore deposits, *J. Volcanol. Geotherm. Res.*, 57, 85-124, 1993
- Mahood, G.A., Geological evolution of a Pleistocene rhyolitic centre, Sierra La Primavera, Jalisco, Mexico, *J. Volcanol. Geotherm. Res.*, 8, 199-230, 1980
- Marti, J., G.J. Ablay, L T Redshaw, and R.S.J. Sparks, Experimental studies of collapse calderas, *J. Geol. Soc. London*, 151, 919-929, 1994.
- McBirney, A., An historical note on the origin of calderas, *J. Volcanol. Geotherm. Res.*, 42, 303-306, 1990.
- Moore, I., and P. Kokelaar, Tectonic influences in piecemeal caldera collapse at Glen Coe volcano, Scotland, *J. Geol. Soc. London*, 154, 765-768, 1997.
- Moore, I., and P. Kokelaar, Tectonically controlled piecemeal caldera collapse: A case study of Glen Coe volcano, Scotland, *Geol. Soc. Am. Bull.*, 110, 1448-1466, 1998.
- Mori, J , and C. McKee, Outward dipping ring-fault structure at Rabaul caldera as shown by earthquake locations, *Science*, 235, 193-195, 1987.
- Mouginis-Mark, P.J., and M.S. Robinson, Evolution of the Olympus Mons caldera, Mars, *Bull. Volcanol.*, 54, 347-360, 1992.
- Nappi, G., A. Renzulli, and P. Santi, Evidence of incremental growth in the Vesuvian calderas (central Italy), *J. Volcanol. Geotherm. Res.*, 47, 13-31, 1991.
- National Coal Board, *Subsidence Engineers Handbook*, 111 pp., London, 1975.
- Newhall, C.G., and D. Dzurisin, Historical unrest at large calderas of the world, *U.S. Geol. Surv. Bull.*, 1855, 1108 pp., 1988.
- Oftedahl, C., Cauldrons of the Permian Oslo rift, *J. Volcanol. Geotherm. Res.*, 3, 343-371, 1978.
- Ono, K., K. Watanabe, M. Komazawa, and S. Watanabe, The structure of Aso caldera, western Japan, as inferred from gravity data, paper presented at 29th International Geological Congress, Kyoto, Japan, 1992.
- Orsi, G., S. De Vita, and M. di Vito, The restless resurgent Campi Flegrei nested caldera (Italy): Constraints on its evolution and configuration, *J. Volcanol. Geotherm. Res.*, 74, 179-214, 1996.
- Pitcher, W.S., The anatomy of a batholith, *J. Geol. Soc. London*, 135, 157-182, 1978.
- Price, N.J., and J.W. Cosgrove, *Analysis of Geological Structures*, 502 pp., Cambridge Univ. Press, New York, 1990.
- Ramberg, H., *Gravity, Deformation and the Earth's Crust. In Theory, Experiments and Geological Application*, 2nd ed., 452 pp., Academic, San Diego, Calif., 1981.
- Reynolds, D.L., Calderas and ring complexes, *Verh. K. Ned. Mijnbouw. Genoot.*, *Geol. Ser.*, 16, 355-379, 1956.
- Richey, J.E., Tertiary ring structures in Britain, *Trans. Geol. Soc. Glasgow*, 19, 42-140, 1932.
- Ritter, S.P., and J.C. Cepeda, The Hechiceros caldera: A recently identified mid-Tertiary caldera in eastern Chihuahua, Mexico, *J. Geophys. Res.*, 96(B10), 16241-16250, 1991.
- Rymer, H., B. van Wyk de Vries, J. Stix, and G. Williams-Jones, Pit crater structure and processes governing persistent activity at Masaya volcano, Nicaragua, *Bull. Volcanol.*, 59, 345-355, 1998.
- Rytuba, J.J., Evolution of volcanic and tectonic features in caldera settings and their importance in the localisation of ore deposits, *Econ. Geol.*, 89(8), 1687-1696, 1994.
- Rytuba, J.J., and E.H. McKee, Peralkaline ash flow tuffs and calderas of the McDermitt volcanic field, southeast Oregon and north central Nevada, *J. Geophys. Res.*, 89(B10), 8616-8628, 1984
- Sanford, A.L., Analytical and experimental study of simple geologic structures, *Geol. Soc. Am. Bull.*, 70, 19-52, 1959.
- Sawada, Y., Subterranean structure of collapse caldera associated with andesitic and dacitic eruptions: Structural evolution of the Miocene Kakeya cauldron, southwest Japan, *Bull. Volcanol.*, 47, 551-568, 1984.
- Scandone, R., Chaotic collapse of calderas, *J. Volcanol. Geotherm. Res.*, 42, 285-302, 1990.
- Schultz, R A., Relative scale and the strength and deformability of rock masses, *J. Struct. Geol.*, 18(9), 1139-1149, 1996.
- Seager, W.R., and M. McCurry, The cogenetic Organ cauldron and batholith, south central New Mexico: Evolution of a large volume ash flow cauldron and its source magma chamber, *J. Geophys. Res.*, 93(B5), 4421-4433, 1988
- Self, S., and M.R. Rampino, The 1883 eruption of Krakatau, *Nature*, 294, 699-704, 1981.
- Setterfield, T.N., P.C. Eaton, W.J. Rose, and R.S.J. Sparks, The Tavua caldera, Fiji: A complex Shoshonitic caldera formed by concurrent faulting and down-sagging, *J. Geol. Soc. London*, 148, 115-127, 1991.

- Shaw, H.R., Viscosities of magmatic silicate liquids: An empirical method of prediction, *Am. J. Sci.*, 272, 870-893, 1972.
- Simkin, T., and K.A. Howard, Caldera collapse in the Galapagos Islands, 1968, *Science*, 169, 429-437, 1970.
- Smith, R.B., Ash-flow magmatism, *Spec. Pap. Geol. Soc. Am.*, 180, 5-27, 1979.
- Smith, R.L., and R.A. Bailey, Resurgent cauldrons, *Mem. Geol. Soc. Am.*, 116, 613-662, 1968.
- Spera, F.J., and J.A. Crisp, Eruption volume, periodicity, and caldera area: Relationships and inferences on development of compositional zonation in silicic magmas chambers, *J. Volcanol. Geotherm. Res.*, 11, 169-187, 1981.
- Steven, T.A., and P.W. Lipman, Calderas of the San-Juan volcanic field, southwestern Colorado, *U.S. Geol. Surv. Prof. Pap.*, 958, 35 pp., 1976.
- Suto, S., Piston cylinder type caldera in the Sengan geothermal area, northeast Japan, paper presented at 29th International Geological Congress, Kyoto, Japan, 1992.
- Takahashi, M., Anatomy of a middle Miocene Valles-type caldera cluster: Geology of the Okueyama volcano-plutonic complex, southwest Japan, *J. Volcanol. Geotherm. Res.*, 29, 33-70, 1986.
- Tibaldi, A., and L. Vezzoli, The space problem of caldera resurgence: An example from Ischia island, Italy, *Geol. Rundsch.*, 87, 53-66, 1998.
- Varga, R.J., and B.M. Smith, Evolution of the early Oligocene Bonanza caldera, northeast San Juan volcanic fields, Colorado, *J. Geophys. Res.*, 89(B10), 8679-8694, 1984.
- Vendeville, B., Modèles expérimentaux de fracturation de la couverture contrôlée par des failles normales dans le socle, *C. R. Acad. Sci. Paris, Série II*, 307, 1013-1019, 1988.
- Vidal, V., *Exploitation des Mines*, Dunod, Paris, 1961
- Vincent, P.M., Les volcans tertiaires et quaternaires du Tibesti occidental et central (Sahara et Tchad), *Mém. BRGM*, 23, 247 pp., 1963.
- Vincent, P.M., The evolution of the Tibesti volcanic province, eastern Sahara, in *African Magmatism and Tectonics*, edited by I. G. T. N. Clifford, pp. 301-319, Oliver and Boyd, White Plains, New York, 1970.
- Walker, G.P.L., Downsag calderas, ring faults, caldera sizes, and incremental calderas growth, *J. Geophys. Res.*, 89(B10), 8407-8416, 1984.
- Whittaker, B.N., and D. Reddish, *Subsidence: Occurrence, Prediction and Control*, 528 pp., Elsevier Sci., New York, 1989.
- Williams, H., Calderas and their origin, *Bull.* 25, pp. 239-346, Dep. of Geol. Sci., Univ. of Calif., Berkeley, 1941.
- Wilson, C.J.N., and W. Hildreth, The Bishop Tuff: New insights from eruptive stratigraphy, *J. Geol.*, 105, 407-439, 1997.
- Wood, C.A., Calderas: A planetary perspective, *J. Geophys. Res.*, 89(B10), 8391-8406, 1984.
- Yokoyama, I., Gravity survey on the Aira caldera, Kyushu, Japan, *Nature*, 191, 966-967, 1961.
- Yokoyama, I., A geophysical interpretation of the 1883 Krakatau eruption, *J. Volcanol. Geotherm. Res.*, 9, 359-378, 1981.
- Yokoyama, I., Gravimetric studies and drilling results at the four calderas in Japan, in *Arc Volcanism: Physics and Tectonics*, edited by D. Shimozuru and I. Yokoyama, pp. 29-41, Terra Sci. Pub. Comp., Tokyo, Japan, 1983.
- Yokoyama, I., Funnel-shaped calderas: Evidence from geophysical studies and drillings, paper presented at 29th International Geological Congress, Kyoto, Japan, 1992.
- Yokoyama, I., and S. De la Cruz-Reyna, Comments on "Chaotic collapse of calderas" by R. Scandone, *J. Volcanol. Geotherm. Res.*, 47, 349-357, 1991.
- Yokoyama, I., and M. Mena, Structure of La Primavera caldera, Jalisco, Mexico, deduced from gravity anomalies and drilling results, *J. Volcanol. Geotherm. Res.*, 47, 183-193, 1991.
- Yoshida, T., Tertiary Ishizuki cauldron, southwestern Japan arc: Formation by ring fracture subsidence, *J. Geophys. Res.*, 89(B10), 8502-8510, 1984.

---

T.H. Druitt, O. Merle, and O. Roche, UMR 6524, Université Blaise Pascal, 5 rue Kessler, F-63038 Clermont-Ferrand, France. (roche@opgc.univ-bpclermont.fr)

(Received January 14, 1999; revised July 5, 1999; accepted August 19, 1999.)